CANCER

RING1B recruits EWSR1-FLI1 and cooperates in the remodeling of chromatin necessary for Ewing sarcoma tumorigenesis

Sara Sánchez-Molina[1]*, Elisabet Figuerola-Bou[1], Enrique Blanco[2,3], María Sánchez-Jiménez[1], Pablo Táboas[1], Soledad Gómez[1], Cecilia Ballaré[2,3], Daniel J. García-Domínguez[4], Estela Prada[1], Lourdes Hontecillas-Prieto[4], Ángel M. Carcaboso[1], Óscar M. Tirado[5], Inmaculada Hernández-Muñoz[1,6], Enrique de Álava[4,7], Cinzia Lavarino[1,8], Luciano Di Croce[2,3,9]*†, Jaume Mora[1,8]*†

Ewing sarcoma (EwS) is an aggressive tumor that affects adolescents and young adults. EwS is defined by a chromosomal translocation, EWSR1-FLI1 being the most common, that causes genome reprogramming through remodeling of enhancers. Here, we describe an unexpected function of RING1B, which is highly expressed in EwS. While retaining its repressive activity at Polycomb developmental regulated genes, RING1B colocalizes with EWSR1-FLI1 at active enhancers. We demonstrate that RING1B is necessary for the expression of key EWSR1-FLI1 targets by facilitating oncogene recruitment to their enhancers. Knockdown of RING1B impairs growth of tumor xenografts and expression of genes regulated by EWSR1-FLI1 bound enhancers. Pharmacological inhibition of AURKB with AZD1152 increases H2Aub levels causing down-regulation of RING1B/EWSR1-FLI1 common targets. Our findings demonstrate that RING1B is a critical modulator of EWSR1-FLI1–induced chromatin remodeling, and its inhibition is a potential therapeutic strategy for the treatment of these tumors.

INTRODUCTION

Ewing sarcoma (EwS) is an aggressive, poorly differentiated, human tumor characterized by a chromosomal translocation involving a member of the FET family of genes (*FUS*, *EWSR1* and *TAF15*) and a member of the *ETS* family of transcription factors, with the *EWSR1-FLI1* gene fusion the most common one (*1*). EwS genomes present low mutation rates with *FET-ETS* rearrangements as the dominant genetic aberration in the majority of tumors (*2*). Notably, the cell of origin of EwS is still a controversial field, although human mesenchymal stem cells (hMSCs) and human neural crest stem cells are the most accepted (*3*–*5*).

The EWSR1-FLI1 fusion protein, which contains the transcriptional activation and RNA binding domains of EWSR1 and the DNA binding domain of FLI1, is the main driver of tumorigenesis (*3*, *6*). The resulting fusion oncoprotein has the ability to act as an aberrant transcription factor, leading to gene activation and repression for a well-described set of genes (*3*, *7*). A decade ago, EWSR1-FLI1 was found to bind preferentially to DNA sites containing GGAA microsatellite repeats (*8*, *9*). Recent studies have reported that binding of EWSR1-FLI1 multimers to GGAA repeats acts as a pioneer factor and induces the formation of de novo active enhancers by recruiting the acetyl transferases CBP/p300, E2F3, and the BRG1/BRM-associated factor chromatin remodeling complex (*10*–*12*). On the other hand, it was hypothesized that monomeric EWSR1-FLI1 inhibits transcription at enhancers by displacing endogenous ETS transcription factors from GGAA motifs (*10*). Therefore, the mechanisms by which EWSR1-FLI1 acts as either a gene activator or repressor depend on both DNA sequence and cofactors.

Several proteins from the Polycomb group (PcG) have previously been implicated in EwS tumorigenesis. PcG was first described in *Drosophila melanogaster* as a key regulator of Hox genes expression. PcG proteins not only prevent differentiation by repressing lineage-specific genes but also mark bivalent chromatin regions for subsequent activation. EZH2 (the enzymatic subunit of PRC2) methylates histone H3 at lysine 27 (H3K27me3), while RING1B (the enzymatic subunit of PRC1) ubiquitinates H2A at lysine 119 (H2Aub), both considered repressive histone marks (*13*).

The canonical PRC1 complex (defined by the presence of four subunits, comprising one variant each of PCGF, PHC, CBX, and RING1) has mostly been associated with maintaining gene repression. However, increasing evidence indicates that PRC1 complexes containing RING1B have the potential for transcription activation, via their catalytic-independent association with UTX, an H3K27me3 demethylase, and p300 acetyltransferase (*14*, *15*). With respect to EwS, it was recently shown that EZH2 blocks endothelial and neuroectodermal differentiation (*16*), BMI1 promotes tumorigenicity (*17*), and RING1B represses the nuclear factor κB pathway (*18*). The molecular mechanisms behind the contribution of PcG to EwS have not been addressed. Notably, the GGAA repeats are significantly decorated with H3K27me3 in H1 human embryonic cell lines and human umbilical

[1]Developmental Tumor Biology Laboratory, Institut de Recerca Sant Joan de Déu, Esplugues de Llobregat, 08950 Barcelona, Spain. [2]Center for Genomic Regulation (CRG), Barcelona Institute of Science and Technology, 08003 Barcelona, Spain. [3]Universitat Pompeu Fabra (UPF), 08002 Barcelona, Spain. [4]Instituto de Biomedicina de Sevilla (IBiS), Hospital Universitario Virgen del Rocio/CSIC/Universidad de Sevilla-CIBERONC, Department of Pathology, 41013 Seville, Spain. [5]Sarcoma Research Group, Laboratori d'Oncologia Molecular, Institut d'Investigació Biomèdica de Bellvitge (IDIBELL)-CIBERONC, L'Hospitalet de Llobregat, 08908 Barcelona, Spain. [6]Fundació Institut Hospital del Mar d'Investigacions Mèdiques (FIMIM), 08003 Barcelona, Spain. [7]Department of Normal and Pathological Cytology and Histology, School of Medicine, University of Seville, 41009 Seville, Spain. [8]Pediatric Cancer Center Barcelona (PCCB), Hospital Sant Joan de Déu, Esplugues de Llobregat, 08950 Barcelona, Spain. [9]Institucio Catalana de Recerca i Estudis Avançats (ICREA), Pg Lluis Companys 23, 08010 Barcelona, Spain.
*Corresponding author. Email: ssanchez@fsjd.org (S.S.-M.); luciano.dicroce@crg.es (L.D.C.); jmora@sjdhospitalbarcelona.org (J.M.)
†These authors contributed equally to this work as co-senior authors.

vein endothelial cells (HUVECs) (*19*). This is in stark contrast with the lack of H3K27me3 mark at EWSR1-FLI1 binding sites in EwS cells (*10*, *11*), thus suggesting a different role of PcG in EwS. Last, comparison between malignant and nonmalignant tissues revealed a misregulation of PcG target genes in EwS (*20*). Together, these findings suggest a potential role of the PcG during the early steps of EwS pathogenesis. Here, we report that RING1B and EWSR1-FLI1 interact and colocalize at the same genomic loci. Notably, we find that RING1B is present at promoters and enhancers of actively transcribed EWSR1-FLI1 target genes. Furthermore, we demonstrate that modulation of RING1B interferes with EWSR1-FLI1 recruitment and with the expression of EWSR1-FLI1 targets, thus unveiling an interdependent cooperation between both proteins.

RESULTS

EWSR1-FLI1 targets PcG-repressed regions in hMSC

Human pediatric MSCs (hpMSCs) have been proposed as a plausible cell of origin for EwS (*21*). Nevertheless primary human endothelial HUVECs share high similarity in gene expression profiles with EwS cells (*22*). Thus, to investigate the potential contribution of epigenetic alteration in the initiation of EwS, we analyzed the role of epigenetic marks in these models and compared to established EwS cell lines. We first analyzed the levels of H3K27me3 and H3K4me3 in the human EwS-derived cell line A673 at several bona fide direct targets of EWSR1-FLI1 (table S1) by chromatin immunoprecipitation followed by quantitative polymerase chain reaction (ChIP-qPCR). Promoter of genes that are transcriptionally activated by EWSR1-FLI1, such as *FCGRT*, *NR0B1*, *CACNB2*, *EZH2*, *IGF1*, *NKX2-2*, and *HOXD11*, was enriched for the H3K4me3 mark, and lacked the H3K27me3 mark, in agreement with previous data (*8*, *20*, *23*, *24*) (fig. S1A). On the other hand, transcriptionally repressed genes, such as *KCNA5* (*25*), were enriched for H3K27me3. We next compared the levels of H3K27me3 and H3K4me3 at the same loci in HUVECs and in hpMSCs. In an apparently reversed situation to the A673 EwS cell line, analysis of those promoters presented strong enrichment for H3K27me3 but not for H3K4me3 (fig. S1B). Accordingly, infection of HUVECs with the EWSR1-FLI1 oncogene (Fig. 1A) not only led to the activation of these targets (*FCGRT*, *NR0B1*, *CACNB2*, *EZH2*, *IGF1*, *NKX2-2*, and *HOXD11*) (Fig. 1B) but also decreased the levels of H3K27me3 (Fig. 1C). This demonstrates that, although H3K27me3 is not present at oncogene binding regions in EwS cell lines such as A673, these regions are repressed by PcG before oncogene expression.

To explore the chromatin and transcriptional states of EWSR1-FLI1 binding sites (*10*), we measured the frequency of each chromatin state at these regions (*26*) and compared to the corresponding value obtained for the whole genome in several cell lines [HUVECs, H1, and H9 human embryonic cells, H1-derived MSCs, bone marrow (BM)–derived MSCs, and adipose-derived MSCs]. This analysis indicated that EWSR1-FLI1 binding sites are overrepresented in chromatin states associated with zinc finger genes and repeats (ZNF/repeats) and active promoters (Fig. 1D and table S1). In cells with MSC origin (such as H1, adipose, and BM-derived cell lines), EWSR1-FLI1 binding sites are overrepresented in PcG weak repressed state, which represents flanking regions of H3K27me3 peaks summit (Fig. 1D and fig. S1, C and D). Similar results were obtained when we grouped chromatin states of similar categories (Fig. 1E). This suggests that EWSR1-FLI1 occupies flanking regions of H3K27me3 summit peaks in hMSC, which are considered to be the potential cell of origin for EwS.

Data from our group have revealed that the PRC1 subunit RING1B, is highly overexpressed in EwS primary tumors (*18*). We thus assessed whether RING1B modulates the growth rate of EwS cells as has been reported for other PcG subunits, such as EZH2 and BMI1 (*16*, *17*). RING1B depletion caused a reduction in cell viability in the A673, SK-ES1, and, with a lesser extent, in A4573 EwS cell lines but not in the control cell line 293T (Fig. 1F and fig. S1E), suggesting that RING1B represents an epigenetic vulnerability for EwS cells.

RING1B colocalizes genome-wide with EWSR1-FLI1 at active enhancers

Chan *et al.* (*27*) recently proposed that RING1B might play a role in modulating enhancer activity. Together with its role in promoter regulation, EWSR1-FLI1 has been recently reported to generate de novo enhancers (*10*). This led us to postulate whether EWSR1-FLI1 and RING1B might cooperate during EwS tumorigenesis. We first aimed to define the genome-wide localization of RING1B and its repressive histone mark H2Aub in the A673 cell line by chromatin immunoprecipitation sequencing (ChIP-seq). In two independent experiments, we identified 2573 and 3945 peaks of RING1B, and 26424 and 10269 peaks of H2Aub. Using differential binding analysis (DiffBind), which allows for the identification of statistically common peaks (*28*), we found 2459 RING1B and 5392 H2Aub significant peaks between duplicates ($P < 0.05$, fig. S2A), corresponding to 1264 target genes and 3013 target genes, respectively (table S2). Genomic distribution of peaks showed that RING1B is more abundant in intergenic regions, whereas H2Aub is mainly located in promoters (Fig. 2A). Moreover, 38% of RING1B peaks were found at intergenic regions with respect to 21.5% of H2Aub peaks, and 29.2% of RING1B peaks were in promoters with respect to 40.5% of H2Aub peaks, further supporting the potential role of RING1B at enhancers. We then categorized peaks for RING1B, H2Aub, and EWSR1-FLI1 in active or poised enhancers, and in active or poised promoters, based on H3K27me3, H3K4me3, H3K27ac, and H3K4me1 (*29*). To complement the above data, we performed a ChIP-seq analysis using a different antibody directed against FLI1 (fig. S2B and table S2). We found that an important fraction of RING1B peaks (35%) and EWSR1-FLI1 (46%) are located at transcriptionally active enhancers and promoters of A673 cells (Fig. 2B, left). On the other hand, as expected, 35% of RING1B peaks and 37% of H2Aub peaks showed a preference for transcriptionally repressed regulatory regions (Fig. 2B, left). We then intersected the list of genes associated to RING1B and H2Aub peaks with published data of EWSR1-FLI1 target genes in A673 cells, producing a common set of 162 genes (fig. S2C and table S3). Comparing this set with 386 genes containing only RING1B and H2Aub or the group of 324 EWSR1-FLI1/RING1B genes without H2Aub confirmed that the presence of EWSR1-FLI1 correlated with higher level of transcription ($P < 10^{-16}$; fig. S2D, left). Functional analysis of the common gene set of 324 EWSR1-FLI1/RING1B genes (table S3) returned Gene Ontology (GO) categories related to chondrocyte and neuronal differentiation (fig. S2D, right). EWSR1-FLI1/RING1B/H2Aub genes were also enriched in neuronal differentiation category, while the RING1B/H2Aub genes were related to general transcription. These data suggest that RING1B is a positive regulator of a specific set of genes implicated in EwS and that this activity is independent of its canonical repressive mark.

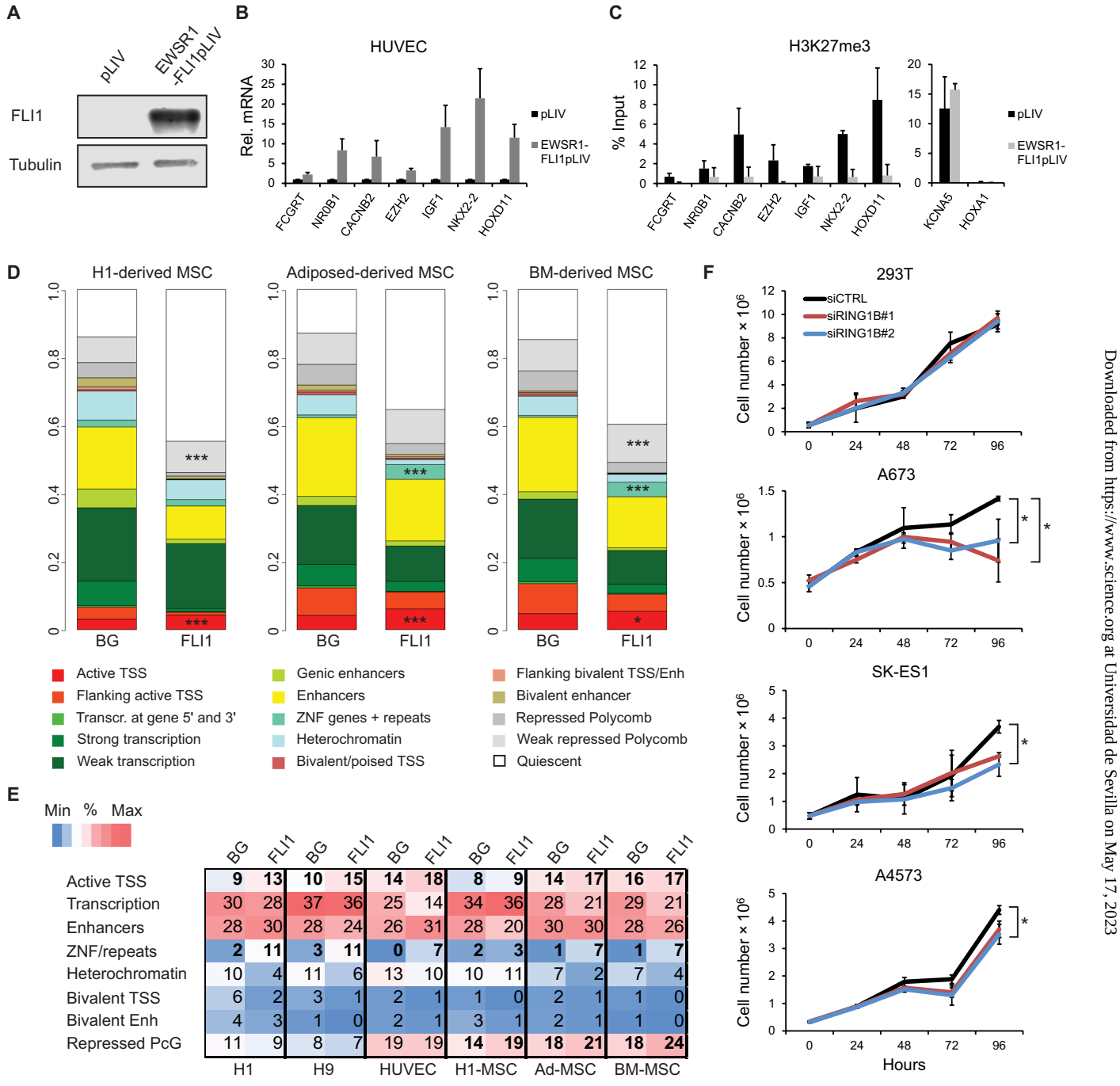

Fig. 1. EWSR1-FLI1 targets PcG-repressed regions in hMSC. (**A**) Western blot showing ectopic expression of EWSR1-FLI1 upon infection of HUVECs with an empty pLIV vector or EWSR1-FLI1pLIV. (**B**) RT-qPCR determination of relative mRNA expression of EWSR1-FLI1 target genes upon infection of HUVECs with an empty pLIV vector or EWSR1-FLI1pLIV. Values are normalized to *TBP*. (**C**) H3K27me3 ChIP-qPCR at EWSR1-FLI1 target gene promoters in HUVECs infected with an empty pLIV vector or EWSR1-FLI1pLIV. The values of the *Y* axis represent the enrichment ratio of immunoprecipitated samples relative to input with subtracted immunoglobulin G (IgG). (**D**) Bar plots of chromatin state relative frequencies in the whole genome [background (BG)] and in published EWSR1-FLI1 binding sites (FLI1) for three selected cell lines. Genome segmentations were extracted from the Epigenome Roadmap Consortium. (**E**) Heatmap with percentages of each chromatin state in the whole genome (BG) as compared to the frequency within published EWSR1-FLI1 binding regions for indicated cell lines by grouping in 8 similar chromatin states the initial classification containing 15 (quiescent segments were excluded). Bold format indicates enrichments greater than 10%. Enrichment scores were calculated as the difference between the value in EWSR1-FLI1 and the value at the whole genome, normalized by the value at the whole genome. (**F**) Cell proliferation expressed as cell number in 293T, A673, SK-ES1, and A4573 cells transiently transfected with small interfering RNA (siRNA) against a control (siCTRL) or two different RING1B sequences (siRING1B#1 and #2). Error bars in (B), (C), and (F) indicate SD of three biological independent experiments. Statistical significance in (D) and (F) is as follows: ***$P < 0.001$ and *$P < 0.05$.

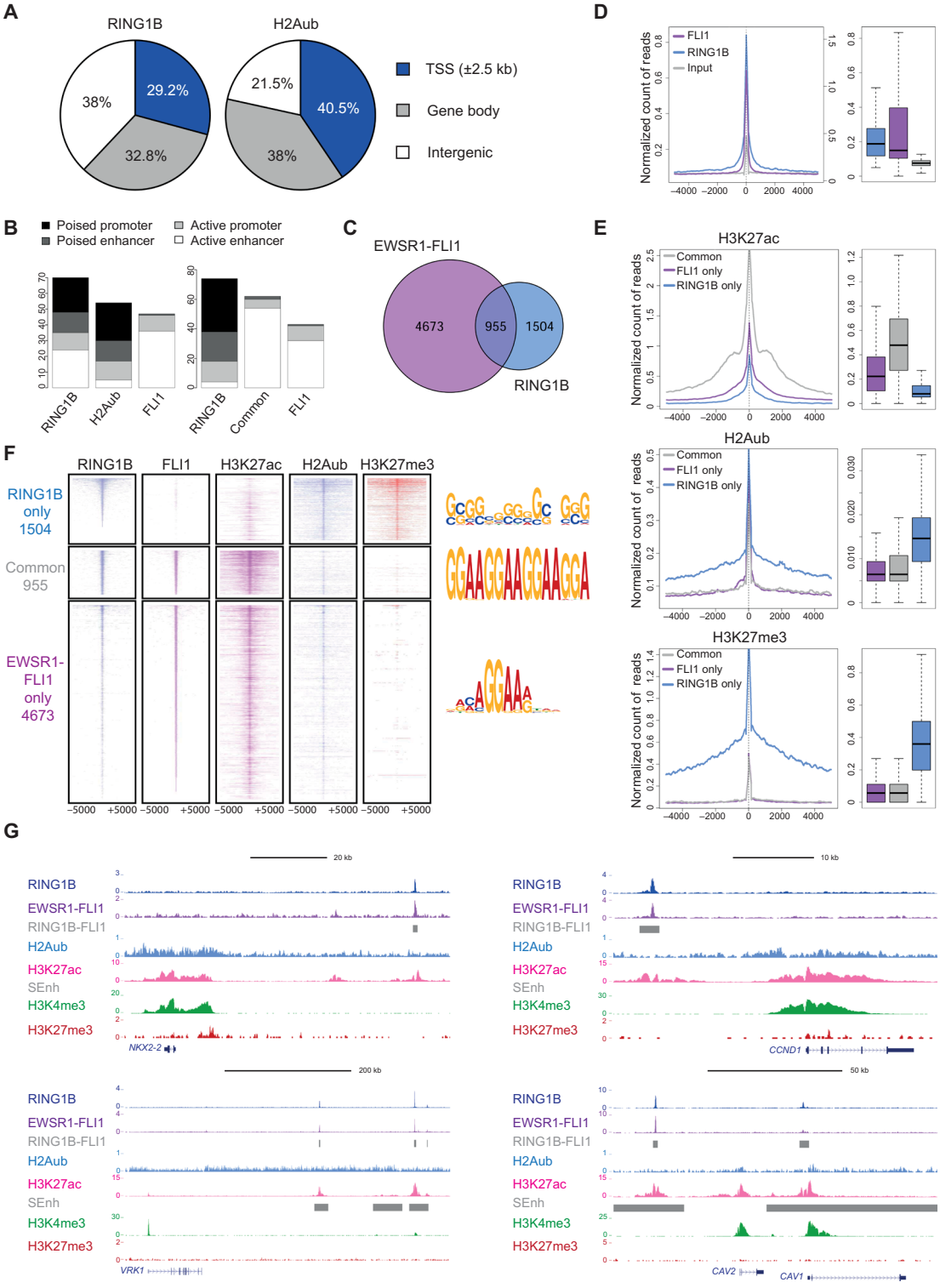

Fig. 2. RING1B colocalizes genome-wide with EWSR1-FLI1 at active enhancers. (**A**) Pie chart showing genomic distribution of RING1B and H2Aub peaks relative to functional categories including promoter (±2.5 kb from TSS), gene body (intragenic region not overlapping with promoter), and intergenic (rest of the genome). (**B**) Boxplot depicting percentage of regulatory elements (active/bivalent enhancers and promoters) in each described group. (**C**) Venn diagram depicting the overlap between RING1B and EWSR1-FLI1 in A673 cells at the peak level. (**D**) Aggregated plot showing the average ChIP-seq signal of RING1B and EWSR1-FLI1 at EWSR1-FLI1 binding sites. (**E**) Aggregated plots showing the average ChIP-seq signal of H3K27ac, H2Aub, and H3K27me3 in the three sets of RING1B and EWSR1-FLI1 peaks. (**F**) Heatmap showing RING1B, EWSR1-FLI1, H3K27ac, H2Aub, and H3K27me3 ChIP-seq signals segregating in the three sets of RING1B and EWSR1-FLI1 peaks. Top MEME motif for every group is shown. (**G**) University of California Santa Cruz (UCSC) genome browser ChIP-seq signal tracks for RING1B, EWSR1-FLI1, H2Aub, H3K27ac, H3K4me3, and H3K27me3 at *NKX2-2*, *CCND1*, *VRK1*, and *CAV1* gene promoters and intergenic enhancer regions. Gray boxes represent EWSR1-FLI1 and RING1B colocalization and ES super-enhancers (SEnh; as shown at *VRK1* and *CAV1/2*).

To fully understand the association of RING1B with transcriptional activation in EwS, we intersected EWSR1-FLI1 peaks with those of RING1B and obtained 955 common regions (Fig. 2C). Notably, intersection between H2Aub and RING1B peaks returned only 589 common peaks. Among the 955 overlapping EWSR1-FLI1/RING1B peaks, we inspected for genes containing an enhancer within 100 kb and obtained 1276 genes, of which 235 (18%) were reported to be regulated by EwS super-enhancers (table S4) (*11*). The common targets of RING1B and EWSR1-FLI1 sites were found within active enhancers, while the majority of RING1B peaks not overlapping with EWSR1-FLI1 were located in transcriptionally repressed regulatory elements (Fig. 2B, right). The distribution of RING1B peaks was centered on EWSR1-FLI1 binding sites (Fig. 2D), suggesting that their binding occurs at the same loci. We next assessed the distribution of H3K27ac, H2Aub, and H3K27me3 in genomic regions occupied by EWSR1-FLI1, RING1B, or shared (Fig. 2E). Common peaks were decorated with H3K27ac, lacking H2Aub (Fig. 2, E and F), and presented narrow RING1B peaks located in intergenic or intronic regions (fig. S2E, right). These data suggest that common sites likely represent enhancers. Known EWSR1-FLI1 target genes such as *NKX2-2*, *CCND1*, *VRK1*, or *CAV1* presented an intergenic peak of RING1B, which overlaps with defined super-enhancers in the case of *VRK1* and *CAV1* (Fig. 2G). Intronic enhancers such as *JARID2* or *MYOM2* (fig. S2G) constitute the majority of the 162 common RING1B, EWSR1-FLI1, and H2Aub genes (53% of sites, fig. S2C). On the other hand, RING1B-specific peaks were associated with H3K27me3 and H2Aub (Fig. 2, E and F) and presented a broader distribution [e.g., *HNF1B* and *TAL1* (fig. S2H)] mainly located within promoter or gene body regions (fig. S2E, left). The bivalent marks H3K4me3 and H3K27me3 decorated 63% of the 932 downstream genes associated to RING1B-specific peaks ($P < 10^{-300}$, table S4) (*29*). RING1B–transcription start sites (TSS) do not overlap with EWSR1-FLI1 and are decorated with H2K27me3 and H2Aub, while RING1B-distal sites overlap with EWSR1-FLI1 and with H3K27ac (fig. S2F).

Last, de novo motif analysis revealed that EWSR1-FLI1–specific sites contained predominantly ($P < 10^{-282}$) one single occurrence of the canonical ETS motif GGAA (Fig. 2F). When EWSR1-FLI1 was associated with RING1B, we observed a significant enrichment for multimeric GGAA repeats ($P < 10^{-1072}$) (*10*). Furthermore, RING1B-sepecific sites were enriched for CG sequence, as previously reported ($P < 10^{-176}$) (*30*). Together, we identified two major types of RING1B peaks in EwS: a prominent group with narrow peaks that colocalizes with EWSR1-FLI1 at enhancers of actively transcribed genes and a second group with broader peaks located at promoters, where RING1B is associated with H2Aub.

RING1B regulates the expression of EWSR1-FLI1 activated and repressed targets

To further characterize RING1B binding regions (table S4), we analyzed several EWSR1-FLI1 active promoters (*CAV1*, *FCGRT*, *NR0B1*, *CACNB2*, *FEZF1*, and *KIAA1797*) and enhancers (*CCND1*, *IGF1*, *CAV2*, *JARID2*, *VRK1*, and *NKX2-2*) by ChIP-qPCR. Both groups showed enrichment for RING1B, with stronger signals at enhancers (Fig. 3A). Known repressed targets of the oncogene (e.g., *IGFBP3*, *TGFBR2*, and *LOX*) also showed binding of RING1B. At these repressed promoters, RING1B was accompanied by its canonical repressive mark H2Aub (fig. S3A). We also validated the occupancy of RING1B in EWSR1-FLI1–activated promoters (*CAV1*, *FCGRT*, *NR0B1*, and *FEZF1*) and enhancers (*CCND1*, *CAV2*, *JARID2*, and *VRK1*) in SK-ES1 cells (fig. S3B). Similar to A673 cells, H2Aub correlated with RING1B at promoters of repressed genes (*IGFBP3*, *TGFBR2*, and *LOX*) (fig. S3C). Last, we observed that the PRC1 and PRC2 subunits, BMI1 and EZH2, respectively, were present at repressed promoters but not in active enhancers (fig. S3, D and E), as well as in promoters with broad peaks of RING1B concomitant with H3K27me3 and H2Aub but no EWSR1-FLI1 (e.g., *TAL1*, *IGF1R*, and *HNF1B*) (fig. S3F). Furthermore, genome-wide analysis demonstrated that BMI1 and CBX7 (*31*) subunits of the PRC1 canonical complex colocalize with RING1B only at repressed regions (*TAL1*) as shown in Fig. 3B, while no detectable peaks are present at active enhancers where EWSR1-FLI1 is present (*VRK1*). Thus, while RING1B decorates EWSR1-FLI1–activated promoters and enhancers, it also maintains its canonical role at several oncogene repressed regions, as well as in a subgroup of genes with no EWSR1-FLI1.

To understand whether RING1B behaves as a canonical repressor and/or activator in EwS, we analyzed the expression changes after knocking down RING1B using two different sets of short hairpin RNA (shRNA, seq#1 and seq#2; fig. S4A). The data obtained showed that 71.94 and 63.85% of genes were down-regulated in the A673 and SK-ES1 cell lines, respectively (FC < -1.5, Fig. 3C). This confirms our finding that RING1B acts predominantly as an activator, despite its presence at several EWSR1-FLI1–repressed targets. Furthermore, H2Aub levels remained unchanged after RING1B knockdown (Fig. 3D), while RING1A knockdown produces a notable decrease in H2Aub levels (fig. S4B). These data suggest that RING1B main function in EwS is uncoupled from its ubiquitin ligase activity toward H2A and that RING1A is the main histone H2A mono-ubiquitin ligase. To further elucidate to what extent RING1B cooperates with EWSR1-FLI1 in transcription regulation, we intersected differentially expressed genes in RING1B knockdown cells (absolute FC > 1.25) with those affected by EWSR1-FLI1 knockdown (absolute FC > 1.5) (*10*), obtaining an overlap of 1078 genes. After segregating these data into down- and up-regulated genes, we found that RING1B and EWSR1-FLI1–activated 229 genes and repressed 162 genes (Fig. 3E and table S5). Among the 229 activated genes, we found several developmental genes, including *SOX2*, *SIX3*, *LYAR*, and *KIT*. GO analysis showed regulation of the potassium channel and mechanisms that control actin monomers and filaments as the main categories (fig. S4C), in agreement with previous publications (*25*, *32*). Among the activated genes, *SOX2* and *KIT* harbored RING1B and EWSR1-FLI1 peaks in intergenic and intronic enhancer regions, respectively (fig. S4E). *TGFBR2*, a gene repressed by both EWSR1-FLI1 and RING1B, also contained an intronic enhancer where both proteins colocalized. Notably, the expression of known targets of EWSR1-FLI1, such as *NKX2-2* or *IGF1* (fig. S4D), was just below our logFC cutoff value. Nonetheless, we confirmed by reverse transcription (RT)–qPCR the changes in expression levels of selected repressed and activated genes cobound by EWSR1-FLI1 and RING1B. We noticed that RING1B knockdown causes a significant reduction in the expression levels of those genes where both EWSR1-FLI1 and RING1B were co-occupying enhancer regions (Fig. 3, F and G). The expression of *CAV1*, *NKX2-2*, *SOX2*, *IGF1*, *JARID2*, and *VRK1* was affected in stronger manner upon EWSR1-FLI1 knockdown, indicating that some cofactors could remain when RING1B is depleted (fig. S4F). The effect of RING1B knockdown was less pronounced when both proteins were enriched at promoter regions of active genes (fig. S4, G and H, left). As expected, at those genes where EWSR1-FLI1 acts as a repressor, RING1B knockdown induces a promoter reactivation (fig. S4, G and H, right).

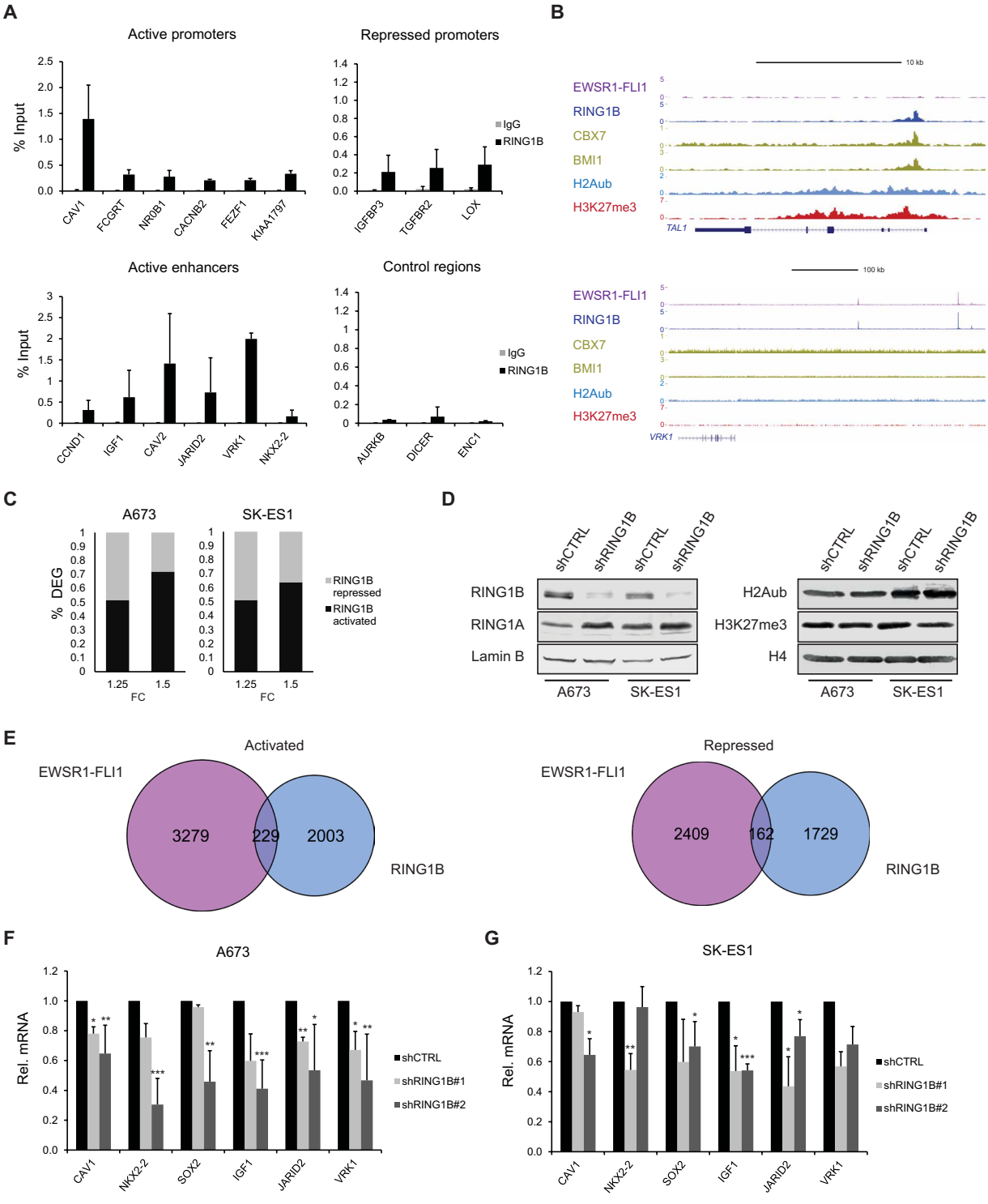

Fig. 3. RING1B regulates the expression of EWSR1-FLI1–activated and EWSR1-FLI1–repressed targets. (**A**) RING1B ChIP-qPCR of EWSR1-FLI1 bound active promoters, repressed promoters, and active enhancers. Control regions indicate the absence of RING1B and EWSR1-FLI1 binding at these sites. The values of the *Y* axis represent the enrichment ratio of immunoprecipitated samples relative to input. (**B**) UCSC genome browser ChIP-seq signal tracks for EWSR1-FLI1, RING1B, CBX7, BMI1, H2Aub, and H3K27me3 at *TAL1* promoter and *VRK1* enhancer. (**C**) Histogram depicting percentages of activated and repressed genes in A673 and SK-ES1 cells with stable RING1B knockdown seq#2 (shRING1B#2) versus control seq#2 (shCTRL#2), with $P < 0.05$ and an absolute fold change (FC) > 1.25 or 1.5. (**D**) Western blot showing RING1B, RING1A, H2Aub, and H3K27me3 in A673 and SK-ES1 cells with either shCTRL#2 or shRING1B#2. Lamin B and histone H4 are used as loading controls. (**E**) Venn diagram showing intersection between differentially activated or repressed genes for EWSR1-FLI1 and RING1B in A673 cells; $P < 0.05$. (**F**) RT-qPCR determination of mRNA expression of EWSR1-FLI1 target genes with active enhancers in shCTRL and shRING1B A673 cells (#1 and #2). Values are normalized to *GAPDH*. (**G**) Same analysis as in (F) for SK-ES1 cells. Error bars in (A), (F), and (G) indicate SD of four independent biological experiments and $^{***}P < 0.001$, $^{**}P < 0.01$, and $^{*}P < 0.05$.

Overall, these data indicate that RING1B and EWSR1-FLI1 cooperate in gene activation, at both the promoter and enhancer levels, while RING1B retains its canonical role at those targets repressed by the oncogene. Since a large number of EWSR1-FLI1 and RING1B co-targets were not altered by RING1B knockdown, we postulate compensatory mechanism(s) or additional cofactors involved in their regulation.

RING1B interacts with EWSR1-FLI1 and affects its recruitment to chromatin

Wild-type EWSR1 interacts with RING1B in the VCaP prostate cancer cell line (*33*). We also confirmed this interaction in SK-ES1 cells (Fig. 4A). Since RING1B and EWSR1-FLI1 are enriched at transcriptionally active regions, we next aimed to investigate whether both proteins interact. Coimmunoprecipitation experiments in HeLa cells where EWSR1-FLI13xFlag was overexpressed (*34*) confirmed that indeed oncogene interacts with RING1B (Fig. 4, B and C). Analysis of published mass spectrometry data demonstrated that several SWI/SNF subunits interact with RING1B (*33*), further supporting an active role of RING1B in EwS gene regulation. Together, our results indicate that EWSR1-FLI1 and RING1B not only colocalize at the same genomic regions but also physically interact, mainly through the EWSR1 component of the fusion protein.

Next, we analyzed whether RING1B depletion affects the EWSR1-FLI1 recruitment to chromatin. As expected, after knockdown, we observed a notable reduction of RING1B in the chromatin bound fraction (Fig. 4D). EWSR1-FLI1 was also evicted from chromatin bound and enriched in the soluble chromatin fraction (Fig. 4D). We then monitored the occupancy of EWSR1-FLI1, RING1B, and H3K27ac at several enhancers (e.g., *SOX2*, *NKX2-2*, and *IGF1*). The data in Fig. 4E showed that upon RING1B knockdown, enrichments at those enhancers decreased to control values [immunoglobulin G (IgG) or *ENC1* region]. To assess the decrease of EWSR1-FLI1 recruitment genome-wide, we performed ChIP-seq analysis of RING1B and FLI1 in shCTRL and shRING1B A673 cells. The analysis indicated that upon RING1B depletion, EWSR1-FLI1 binding to chromatin was reduced (Fig. 4, F and G). In sum, we conclude that in EwS, RING1B exerts its main role as activator by promoting recruitment of EWSR1-FLI1 to enhancer regions.

RING1B knockdown decreases tumor growth in vivo

RING1B stimulates tumor growth and metastasis in melanoma, leukemia, and breast cancers (*14*, *27*). We observed a reduction in colony number when RING1B is depleted in the SK-ES1 cell line (fig. S5A). To gain functional insight into the cancer pathways potentially modulated by RING1B, we performed gene set enrichment analysis (GSEA) by comparing SK-ES1 shCTRL versus shRING1B cells. The top 10 most significant pathways included interferon-α, epithelial-to-mesenchymal transition, hedgehog signaling, and angiogenesis, with a 0.25 *Q* value cutoff (fig. S5B). In EwS, disruption of angiogenic pathways has been described (*4*, *22*). Further inspection of angiogenic gene list revealed that key genes such as *PDGFA*, *FGFR1*, *SLCO2A1*, *CXCL6*, and *S100A4* were down-regulated upon RING1B depletion (fig. S5C).

To assess the relevance of RING1B in vivo, we generated xenografts by injecting SK-ES1 shCTRL or shRING1B cells (seq#1 and seq#2) subcutaneously into athymic nude mice. Cells with reduced RING1B levels showed delayed engraftment and slower tumor growth (Fig. 5A). At 21 days after injection, tumors derived from shRING1B cells were significantly smaller than those from control cells (fig. S5D). Notably, the median survival increases from 26 days for shCTRL cells to 30 days for shRING1B seq#1 and from 20 to 27 days for shRING1B seq#2 (Fig. 5B). Immunohistochemical analyses of tumors confirmed reduced levels of RING1B, while the ES marker CD99 remained essentially unchanged (Fig. 5C and fig. S5E). Furthermore, shCTRL tumors displayed higher proliferation rates than shRING1B, as shown by Ki-67 staining (Fig. 5C).

To better characterize xenograft derived tumors, we performed RNA sequencing (RNA-seq) of a cohort of tumors (six for each group, Fig. 5D). GSEA analysis confirmed the enrichment of angiogenic genes in the shCTRL tumors (fig. S5, F and G). Since RING1B retains its repressive function at several promoters, we hypothesized that the delay in survival and in tumor growth upon RING1B knockdown could be related to up-regulation of tumor suppressor genes (TSG). GSEA applied to 983 genes from TSG database (https://bioinfo.uth.edu/TSGene), indicated that this gene list was enriched in shCTRL phenotype, suggesting that tumor growth and survival differences observed were not due to RING1B repression of TSG (fig. S5H). The *NKX2-2*, *SOX2*, and *IGF1* genes are necessary for EwS tumor proliferation (*21*, *23*, *35*). In agreement, confirmed *RING1B* and *EWSR1-FLI1* expression reduction (Fig. 5E) is associated to down-regulation of these genes in xenograft tumors (Fig. 5F, left), as we previously shown in EwS cells (Fig. 3, F and G). Furthermore, after RING1B knockdown, we also validated down-regulation of *S100A4*, *SLCO2A1*, and *VEGFA*, which are main activators of angiogenic signaling pathways (Fig. 5F, right). All these data highlight the role of RING1B as an activator in EwS tumorigenesis.

EWSR1-FLI1/RING1B targets are regulated by AURKB inhibition

Several kinases (including AURKB, MEK1, and CK2) have been reported to modulate the activating transcriptional function of RING1B (*14*, *15*, *36*). To investigate which pathway(s) regulates RING1B at active enhancers in EwS, we analyzed the expression levels of these three kinases in a publicly available database (*4*) comprising a cohort of 27 tumor samples and BM-MSCs. While *MEK1* and *CK2* were not expressed in primary tumors with respect to BM-MSCs (control), 11 of 27 EwS tumors (40%) showed higher levels of *AURKB* compared to control (fig. S6A). EWSR1-FLI1 directly regulates the expression of *AURKB* (*37*), as also demonstrated by *AURKB* down-regulation in EwS cell lines upon oncogene knockdown (fig. S6A).

AZD1152 is a specific AURKB inhibitor, with a median inhibitory concentration (IC_{50}) of 19 nM in EwS cell lines (*38*). Accordingly, we observed IC_{50} values of 5 and 6 nM in SK-ES1 and A4573 cells, respectively; in contrast, the IC_{50} for A673 was 5 μM, and AZD1152 had no effect on the control cell line 293T (fig. S6B). EwS cells that survived to the treatment showed an atypical phenotype, suggesting enhanced differentiation (fig. S6C). Furthermore, viability of EwS cell lines was not affected by the inhibition of RING1B E3 ubiquitin ligase activity with PRT4165 (fig. S6B). To further elucidate the effect of AZD1152 in EwS, cell death was analyzed by Annexin V staining. A 72-hour AZD1152 treatment of A673, SK-ES1, and A4573 cells led to an increase in the early and late apoptosis populations as compared to 293T cells (Fig. 6A). Analysis of cleaved PARP levels further demonstrated that AZD1152 stimulated apoptotic pathways in EwS cell lines, with SK-ES1 being the most sensitive (Fig. 6B). It is worth noting that the levels of EWSR1-FLI1 were decreased after AZD1152 treatment in SK-ES1

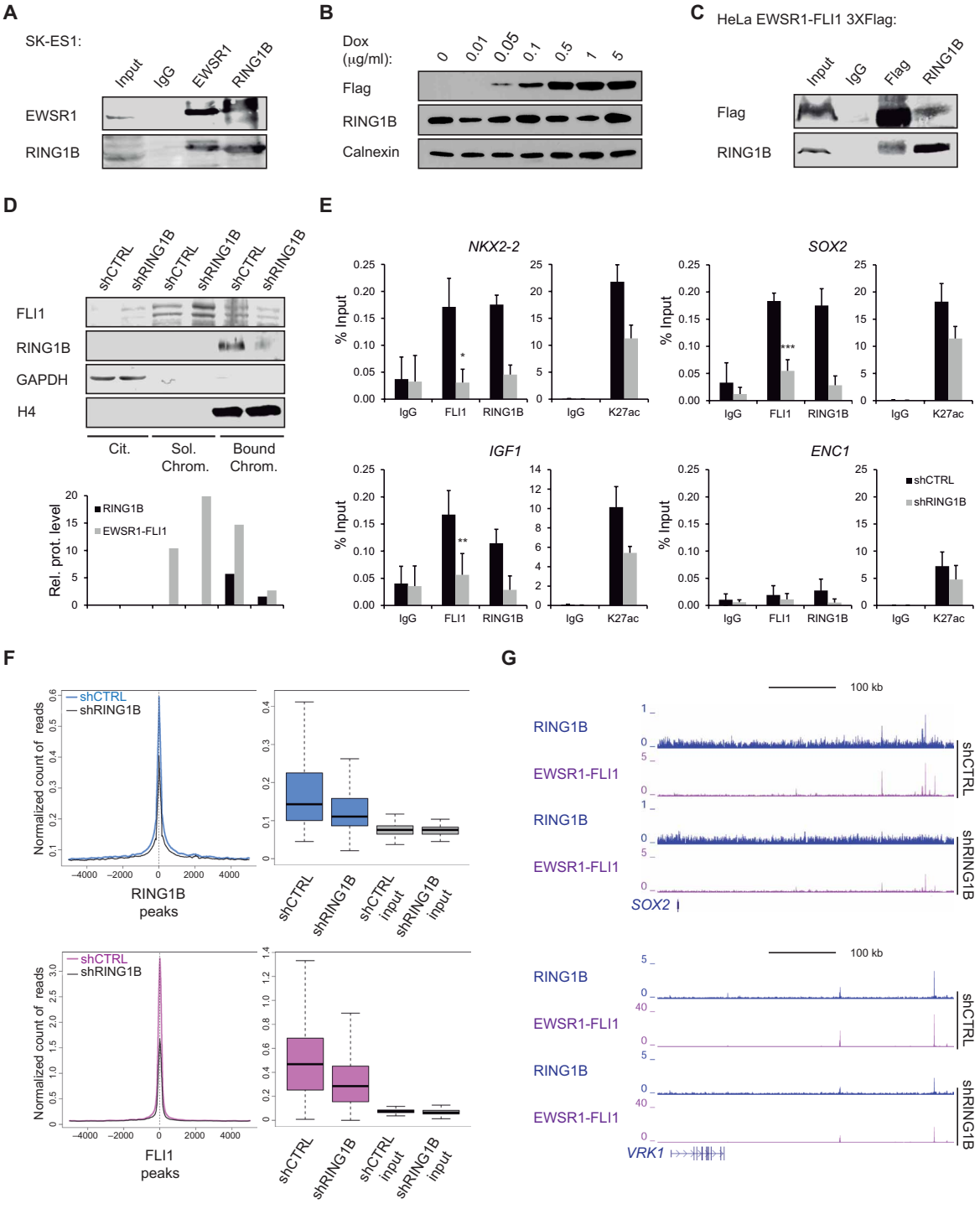

Fig. 4. RING1B interacts with EWSR1-FLI1 and affects its recruitment to chromatin. (**A**) Western blot showing endogenous coimmunoprecipitation of RING1B with EWSR1 in the SK-ES1 cell line. (**B**) Western blot showing overexpression of EWSR1-FLI1-3xFlag and RING1B levels in HeLa stably transfected cells upon induction with indicated doxycycline concentrations for 24 hours. Calnexin is used as loading control. (**C**) Coimmunoprecipitation of RING1B with EWSR1-FLI1-3xFlag under induction conditions (0.5 μg/ml). Inputs in (A) and (C) contain 10% of immunoprecipitated material and IgG is used as control. (**D**) Western blot showing RING1B and EWSR1-FLI1 in cytoplasm, soluble, and bound chromatin fractions in shCTRL#1 or shRING1B#1 SK-ES1 cells. Histone H4 is used as a control of bound chromatin, and GAPDH as a control of cytoplasmic fraction. Blot quantification of the same ordered samples is depicted below. (**E**) ChIP-qPCR analysis of FLI1, RING1B, and H3K27ac at EWSR1-FLI1–activated enhancers of *NKX2-2*, *SOX2*, or *IGF1* genes in shCTRL#2 and shRING1B#2 A673 cells. *ENC1* is used as negative control region. The values of the *Y* axis represent the enrichment ratio of immunoprecipitated samples relative to input. Error bars indicate SD of three independent biological experiments. Statistical significance is as follows ***$P < 0.001$, **$P < 0.01$, and *$P < 0.05$. (**F**) Aggregated plot and boxplot showing the average ChIP-seq signal of RING1B and FLI1 peaks at RING1B and EWSR1-FLI1 binding sites, respectively, in shCTRL#2 and shRING1B#2 A673 cells. (**G**) UCSC genome browser ChIP-seq signal tracks for EWSR1-FLI1 and RING1B in shCTRL#2 and shRING1B#2 A673 cells at *SOX2* and *VRK1* enhancer regions.

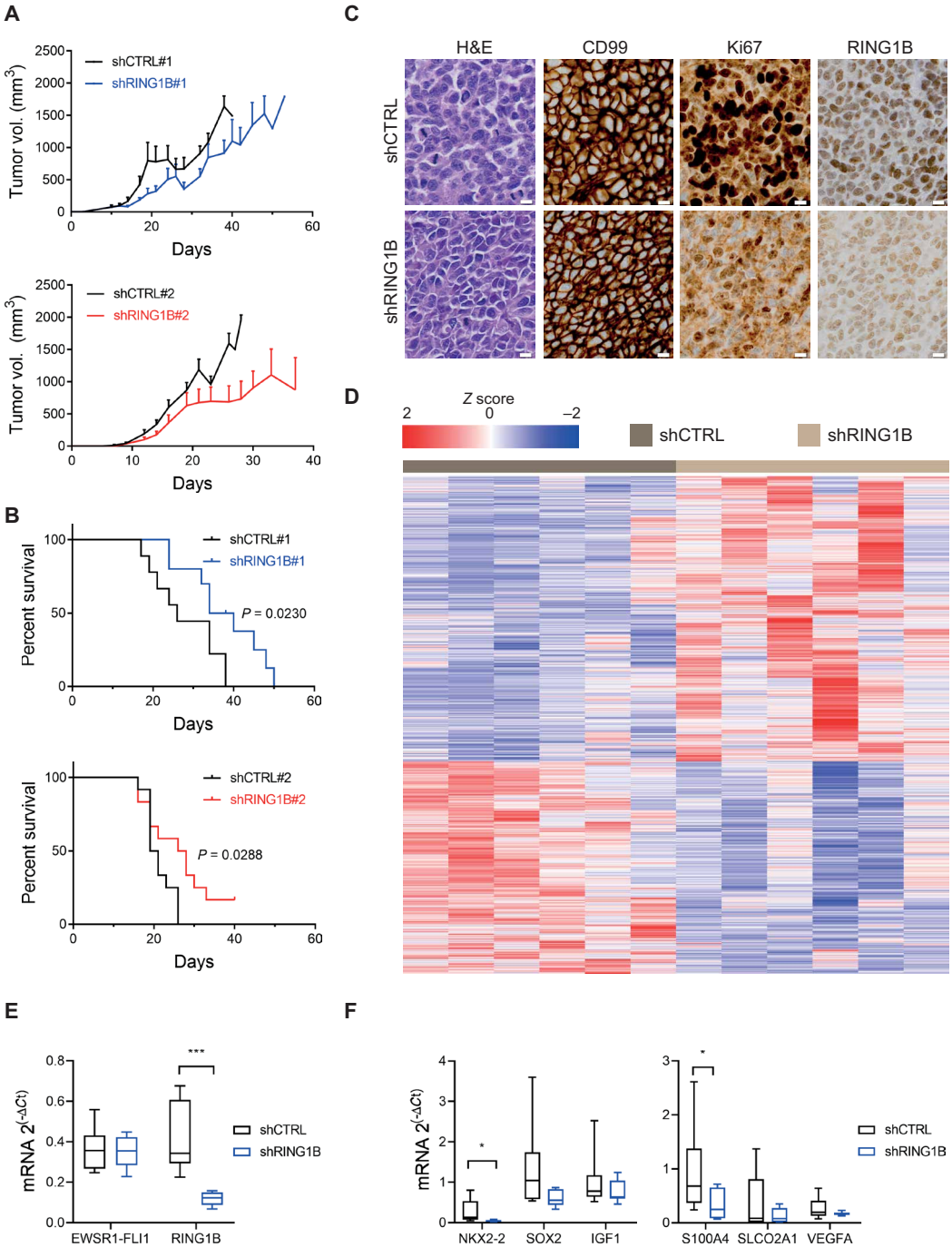

Fig. 5. RING1B knockdown decreases tumor growth in vivo. (**A**) Tumor volume curve in xenografts established by subcutaneous injection of shCTRL and shRING1B#1 ($n = 9$ and $n = 10$, respectively, above) or shRING1B#2 ($n = 12$ both groups, below) SK-ES1 cells in athymic nude mice. (**B**) Kaplan-Meier xenograft survival curves in shCTRL and shRING1B SK-ES1 cells (#1 and #2). (**C**) Immunohistochemistry staining of EWSR1-FLI1, CD99, and RING1B on sections of tumors excised from shCTRL#1 and shRING1B#1 SK-ES1 xenografts. Proliferation was analyzed by Ki67 immunohistochemistry; hematoxylin and eosin (H&E) was used as control. (**D**) Heatmap depicting fold changes in gene expression in six tumors excised from shCTRL#1 and shRING1B#1 SK-ES1 groups. (**E**) RT-qPCR levels of mRNA expression for *RING1B* and *EWSR1-FLI1* in shCTRL#1 and shRING1B#1 SK-ES1–derived tumors; ***$P < 0.001$. (**F**) RT-qPCR levels of mRNA expression for genes regulated by EWSR1-FLI1/RING1B enhancers (left) and angiogenic genes (right) in shCTRL#1 and shRING1B#1 SK-ES1 derived tumors; *$P < 0.05$.

and A4573, yet RING1B levels were unaffected (Fig. 6B and fig. S6, D and E, right). To understand how AURKB modulates RING1B in EwS, we analyzed H2Aub levels after AZD1152 treatment. We observed increased levels of H2Aub repressive mark after AURKB inhibition, suggesting that this kinase indeed inhibits the ubiquitin ligase activity of RING1B in EwS (Fig. 6C). Furthermore, in SK-ES1 and A4573 cells, the increase in ubiquitin ligase activity correlated with decreased expression of EWSR1-FLI1 targets co-occupied by

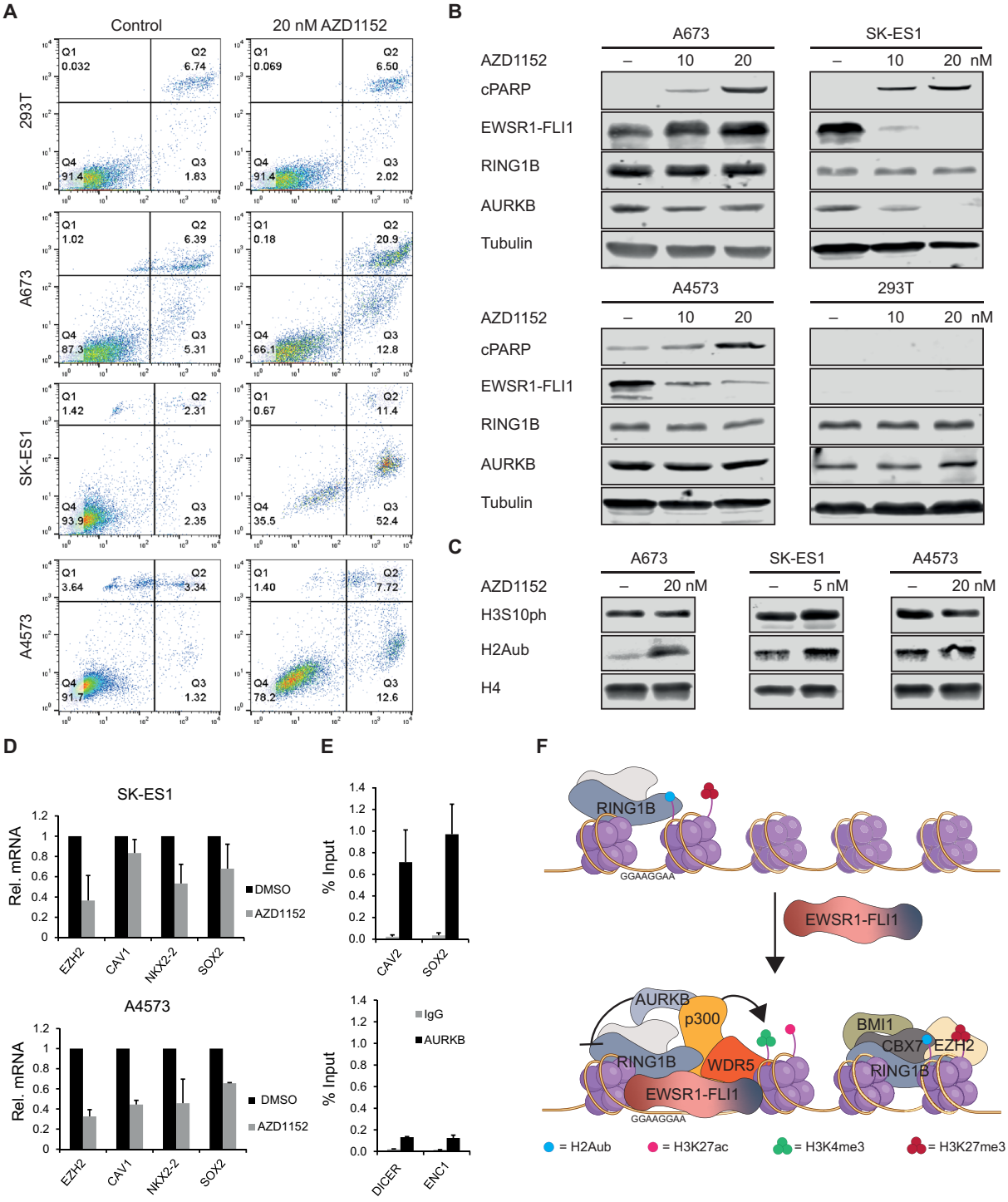

Fig. 6. EWSR1-FLI1/RING1B targets are regulated by AURKB inhibition. (**A**) Annexin V staining of SK-ES1, A673, and A4573 cells after treatment with AZD1152 (20 nM). 293T cells were used as a control cell line. (**B**) Western blot analysis of cleaved poly(ADP-ribose) polymerase (cPARP), EWSR1-FLI1, RING1B, and AURKB after treatment with 10 or 20 nM AZD1152, in the A673, SK-ES1, A4573, and 293T cell lines. Tubulin was used as loading control. (**C**) Western blot analysis of H2Aub and H3S10phospho (H3S10ph) in the A673, SK-ES1, and A4573 cell lines treated with 5 or 20 nM AZD1152. Histone H4 was used as loading control. (**D**) RT-qPCR determination of mRNA expression of target genes with RING1B/EWSR1-FLI bound enhancers in SK-ES1 and A4573 cells after treatment with 20 nM AZD1152. *RPL27* was used for normalization. DMSO, dimethyl sulfoxide. (**E**) AURKB ChIP-qPCR at *CAV2* and *SOX2* EWSR1-FLI1/RING1B enhancers (above) and control regions (below). The values of the *Y* axis represent the enrichment ratio of immunoprecipitated samples relative to input. Error bars in (D) and (E) indicate SD of three independent biological experiments. (**F**) Schematic representation illustrating the EWSR1-FLI1 recruitment by RING1B to repressed regions containing GGAA repeats. Once EWSR1-FLI1 has been recruited, additional cooperating factors such as AURKB might inhibit RING1B ubiquitin ligase activity, which, in turn, is able to participate in transcription activation.

RING1B, with more pronounced effect on those genes where both proteins colocalize at the enhancer region (Fig. 6D and fig. S6, D and E, left). For the A673 cell line, higher doses were required to reach oncogene target deregulation, as expected. Next, we reasoned that AURKB should be present at those regions where it inhibits RING1B activity. Using ChIP-qPCR, we demonstrated that AURKB is enriched in active enhancers (*CAV2*, driving *CAV1* expression, and *SOX2*; Fig. 6E) and promoters (*NR0B1*; fig. S6F). Furthermore, *EWSR1-FLI1* down-regulation could be explained by the presence of RING1B at the *EWSR1* promoter, which indirectly decreases upon AZD1152 incubation (fig. S6G). Although part of AZD1152 cytotoxicity might be related to reduction of EWSR1-FLI1 availability, the data presented suggest that RING1B regulation of oncogene targets is susceptible to AURKB inhibition. The translational value of this potential targetable vulnerability is the matter of ongoing work.

DISCUSSION

RING1B in active enhancers

Here, we investigated the genome-wide occupancy of RING1B in EwS. In agreement with previous data, we identified a set of regions bound by RING1B where it exerts its canonical repressive function. We also report that RING1B co-occupy together with EWSR1-FLI1 many intergenic and intronic regions decorated with H3K27ac. A strong enrichment in GGAA repeats has been described in regulatory elements where EWSR1-FLI1 binds producing active enhancers (*10*). The presence of GGAA repeats, as well as the H3K27ac association, indicates that cobinding of RING1B and EWSR1-FLI1 occurs in active enhancers. BMI1 or EZH2 was not found at these enhancer regions, suggesting a Polycomb-independent function for RING1B. Enhancers are key regulatory regions implicated in cell fate determination. Here, we unveiled that an aberrant transcription factor such as EWSR1-FLI1 relies on RING1B to activate enhancers, causing an altered gene expression profile, which favor cell transformation.

Transcription regulation and EWSR1-FLI1 recruitment by RING1B

In accordance with RNA-seq data from melanoma and breast cancer, where a positive association of RING1B with transcription activation has been reported (*14*, *27*), we observed in EwS cells a higher number of genes activated than repressed by RING1B. We found *NKX2-2*, *SOX2*, and *IGF1* being direct targets down-regulated both in vivo and in vitro upon RING1B knockdown. In EwS, *NKX2-2* and *SOX2* are key players in tumorigenesis (*21*, *23*), suggesting that modulation of their expression in vivo upon RING1B knockdown might contribute to decreased tumor volume and better survival, supporting an oncogenic role for RING1B.

Recent studies in hpMSCs have demonstrated that, before oncogene recruitment, H3K27me3 is enriched at regions where EWSR1-FLI1 could bind (*39*). In agreement with these data, we further demonstrate that upon EWSR1-FLI1 expression, those same regions loose H3K27me3 marks while becoming transcribed. Moreover, we report that enrichment in Polycomb repressed chromatin states is specific for H1-, adipose- and BM-derived MSCs, reinforcing hMSC as the putative cell of origin, which has already been described by other groups (*4*, *21*). The existence of H3K27me3 repressed regions decorated only with PRC1 complex has already been described during differentiation of neural precursor cells, where RING1B and PCGF2 are retained while the PRC2 subunit Suz12 is not (*40*). In melanoma, *CCND2* is marked with H3K27me3 before RING1B activation by phosphorylation (*14*). We have observed that GGAA repeats are differentially enriched in the binding motif analysis when RING1B is associated to chromatin with EWSR1-FLI1. In this scenario, given the interaction observed for RING1B and EWSR1-FLI1, it is tempting to speculate that RING1B targets EWSR1-FLI1 to specific sites. In line with this hypothesis, the reduced recruitment of EWSR1-FLI1 to chromatin (including enhancer regions, such as *NKX2-2*, *SOX2*, and *IGF1*) upon RING1B knockdown underlines the importance of RING1B in the initials steps of EwS tumorigenesis. Overall, our data suggest that RING1B is required for the recruitment of EWSR1-FLI1 to multimeric GGAA repeats (Fig. 6F).

Beyond EWSR1-FLI1

We have demonstrated that RING1B is an essential partner of EWSR1-FLI1 triggering chromatin remodeling. Recent studies demonstrated the requirement of SWI/SNF, WDR5, and p300 acetyltransferase for EWSR1-FLI1–induced transcription. Similarly, in synovial sarcoma, the SS18-SSX oncogenic fusion protein and the SWI/SNF complex colocalize at KDM2B-repressed target genes together with the noncanonical PRC1.1 complex to produce transcriptional active regions (*41*). Along the same lines, in leukemia, noncanonical PRC1.1 also targets active genes independently of H3K27me3 (*42*). Further mechanistic insights are needed to elucidate the contribution of PRC1.1 repressive complex in EwS, where somatic mutations in BCOR have been reported (*1*). The noncanonical PRC1.1 complex contains a DNA binding ZnF-CXXC domain able to target chromatin via KDM2B (*43*). ZNF/repeats chromatin state was statistically enriched in five of the six EwS cell lines analyzed.

Recently, different cell models have shown that the E3 ubiquitin ligase activity of RING1B is inactivated by phosphorylation (*15*, *36*). Our results showing the recruitment of AURKB to enhancers are compatible with a model in which RING1B is unable to repress the newly formed ES enhancers, which were previously Polycomb-repressed regions. Once the oncogene binds to chromatin, RING1B would cooperate to induce transcription activation if its ubiquitin ligase activity is inhibited by phosphorylation (either directly or indirectly) (Fig. 6F). More studies are needed to clarify how oncogenic fusion proteins act as binding scaffolds to recruit a specific set of interactors to generate previously unknown functional units (such as neo-enhancers).

Targeting RING1B with AZD1152

Inhibition of super-enhancers activity with BET inhibitors has emerged as a successful preclinical strategy in the fight against different pediatric cancers such as EwS, neuroblastoma, and rhabdomyosarcoma (*44*–*46*). Inhibition of AURKB with AZD1152 increases H2Aub and decreases expression of key oncogene targets, thus suggesting that RING1B is essential for enhancer deregulation by EWSR1-FLI1. Nevertheless, as RING1B account for catalytic and noncatalytic dependencies (*14*), further investigation should address its clinical therapeutic implications. In agreement with our data, combined inhibition of AURKA and AURKB, as well as synergistic activity of AURKB with focal adhesion kinase inhibitors, has been described effective in EwS preclinical studies, although AURKB efficiency as single agent has not been proved (*47*, *48*). In EwS cells, AZD1152 could affect the levels of RING1B, and this likely reverberates on the regulation of the oncogene's promoter since RING1B occupies the *EWSR1* promoter (fig. S6, E and G).

In summary, we demonstrate the oncogenic dependency to high levels of RING1B in EwS. The data support a model in which RING1B plays a pivotal role for EWSR1-FLI1 recruitment to the multimeric DNA repeats. This, in turn, allows for transcriptional activation that defines the characteristic transcriptome of EwS. Given the role of RING1B in the activation of super-enhancers, which are critical elements for cell fate determination, we propose that the EwS cell of origin is predefined by high levels of RING1B.

MATERIALS AND METHODS

Cell culture and cell viability assays

The Ewing's sarcoma cell lines A673, SK-ES1, and A4573, which carry the EWSR1-FLI1 translocation types I, II, and III, respectively, and the HEK293 cell line from human embryonic kidney infected with AgT from SV40 (293T), were cultured in RPMI 1640 media (Gibco) and supplemented with 10% fetal bovine serum, L-glutamine, and penicillin/streptomycin. Cells were cultured at 37°C with 5% CO_2. The A673 and SK-ES1 cell lines harboring shCTRL and shRING1B with seq#1 and seq#2 as well as A673 cell line with doxycycline inducible knockdown of EWSR1-FLI1 were previously described (*11*, *18*). hpMSCs were isolated following published protocols (*21*). Ectopic expression of EWSR1-FLI1 3xFLAG C terminus in HeLa cells was induced with doxycycline (0.5 μg/ml) (*34*).

All experiments performed with AZD1152 were incubated 72 hours, with the exception of RNA expression assays that were incubated 24 hours. For IC_{50} calculations, A673, SK-ES1, A4573, and 293T cell lines were seeded at 2000 cells per well in 96-well culture plates. AZD1152 and PRT4165 (Sigma-Aldrich) was added to complete growth medium; after 72 hours, cells were subjected to the ATPlite assay (PerkinElmer), and measurements were performed using a Tecan plate reader. Inhibitory concentrations were calculated using OriginPro 9.0 software.

Plasmids and small interfering RNA transfection

EWSR1-FLI1 type 2 was amplified from a pSG5 vector with primers containing Bgl II and Hind III sequences (forward, 5′-ggaggaag-g*AGATCT*AATGGCGTCCACGG-3′; reverse, 5′-aag*AAGCTT*GTAG-TAGCTGCCTAA-3′). The PCR product was purified using an Illustra GFX PCR DNA and Gel Band Purification kit (GE Healthcare Life Sciences). The product of the amplification was subcloned into the TOPO TA Cloning Kit for Sequencing following the manufacturer's instructions. TOPO-EWSR1-FLI1 plasmid and the acceptor vector pEGFP-N1 were double digested with Bgl II and Hind III at 37°C. The resulting EWSR1-FLI1 band was ligated into pEGFP-N1, and ligation product was then transformed into JM109 cells.

Target sequences for siRNA are described in table S6. Transfection of small duplexes (Sigma-Aldrich) was performed with Lipofectamine RNAiMAX and Optimem (Invitrogen), using 30 pmol when cells were 80% confluent; samples were collected after a 72-hour incubation. Transient transfections of GFP constructs or empty vector were done using FuGENE XP (Roche) with 1 to 2 μg of plasmid when cells were 60% confluent; samples were collected after 48 hours. Both reagents were used according to the manufacturer's recommendations.

Lentivirus infection

Empty pLIV and EWSR1-FLI1pLIV–expressing lentiviruses were provided by N. Riggi (University Institute of Pathology Lausanne, Switzerland). Lentiviruses were produced in Lenti-X 293T packaging cells (Takara, Cultek) at a low passage number. For each plate, 7 μg of the lentiviral plasmid, 5 μg of the envelope plasmid (VSV-G), and 6 μg of the packaging plasmid (PAX8) were prepared and introduced by calcium phosphate transfection, according to standard protocols. The supernatant containing lentiviruses was collected 48 hours after transfection. The HUVEC cell line was seeded at 3000 cells/cm^2 and transduced with 3:1 of the lentiviral supernatant with fresh media containing Polybrene (Sigma-Aldrich) at 6 μg/ml. Cells were selected with fresh growth media containing puromycin (0.3 μg/ml) for 72 hours. A control dish without the transduction media was also selected with puromycin, to control for killing of nontransduced cells.

Cell extract preparation, immunoprecipitation, and Western blotting

Histone extracts of cultured cells were isolated using the EpiQuick Histone Extraction kit (Epigentek) following the manufacturer's instructions. Total cell extracts were prepared in IPH buffer [50 mM tris-HCl (pH 8), 150 mM NaCl, 5 mM EDTA, and 0.5% NP-40] with EDTA-free protease inhibitor cocktail (Roche). For protein, fractionation standard protocols were used. Histone or total protein extracts were quantified by Bradford assay. Immunoprecipitation was performed with total cellular extracts incubated at 4°C overnight with primary antibody. After incubation of immunoprecipitated samples on protein A/G and agarose beads (Santa Cruz Biotech), 30 to 50 μg of whole protein extracts or 5 μg of histones was resolved by polyacrylamide gel electrophoresis. Western blotting was performed using standard protocols. Incubation with primary antibodies was done at 4°C overnight and LI-COR secondary antibodies that are detectable by near-infrared fluorescence were used for detection (table S6). Blots were scanned with an Odyssey CLx Infrared Imaging System at medium intensities.

Cell cycle analysis and Annexin V staining

Treated cells were fixed in 70% ethanol, stained with 25 μl of propidium iodide (PI) (1 mg/ml), and 25 μl of ribonuclease (RNase) (10 mg/ml), and incubated 30 min at 37°C. For Annexin V binding, the Alexa Fluor 488 fluorophore kit (Invitrogen) was used for apoptotic cell detection. After culture and treatment, cells were resuspended in annexin binding buffer with 5 μl of Alexa Fluor 488 Annexin V and 1 μl of PI working solution (100 μg/ml). After 15 min, samples were run in Gallios multicolor flow cytometer (Beckman Coulter) set up with the 3-lasers, 10 colors standard configuration. Histograms and cytograms were further analyzed with FlowJo 10.2.

RNA extraction and RT-qPCR

Total RNA was isolated and purified from collected cells using the RNeasy Mini Kit (Qiagen) according to the manufacturer's protocol. After quantification using the NanoDrop software (Thermo Fisher Scientific), RT was performed. A 1-μg aliquot of each RNA sample was converted to cDNA in a reaction catalyzed by a retrotranscriptase enzyme (M-MLV Reverse Transcriptase Promega). Random primers and RNase inhibitor (RNasin Plus RNase Inhibitor, Promega) were also added to the reaction. cDNA obtained was analyzed by qPCR using SYBR Green PCR Master Mix (ABI). cDNA was amplified with specific oligonucleotides (table S6). Each cDNA sample was run in triplicate, and its levels were analyzed using the 7500 Fast PCR instrument (Applied Biosystems). To compare between different conditions studied, relative quantification of each target was normalized

to a housekeeping gene. Last, data were analyzed using the comparative $2^{-\Delta\Delta ct}$ method.

Microarray gene expression and RNA-seq

Gene expression microarrays were performed at the Microarray Analysis Service, Hospital del Mar Medical Research Institute (IMIM, Barcelona). RNA samples were amplified, labeled according to a GeneChip WT PLUS Reagent kit, and hybridized to Human Gene 2.0 ST (Affymetrix) in a GeneChip Hybridization Oven 640. Washing and scanning were performed using the Expression Wash, Stain, and Scan Kit and the GeneChip System of Affymetrix (GeneChip Fluidics Station 450 and GeneChip Scanner 3000 7G). After quality control, raw data were background corrected, quantile-normalized, and summarized to a gene level using the robust multichip average; a total of 48,144 transcript clusters, excluding controls, were obtained, which roughly corresponds to genes and other RNAs, such as long intergenic noncoding RNAs and microRNAs. NetAffx 36 annotations, based on the human genome 19, were used to summarize data into transcript clusters and to annotate analyzed data. Linear Models for Microarray (limma), a moderated *t* statistics model, was used for detecting differentially expressed genes between the conditions. All data analyses were performed in R (version 3.4.3) with R/Bioconductor packages aroma.affymetrix, Biobase, affy, limma, genefilter, ggplots, and Vennerable. Genes with a *P* less than 0.05 were selected as significant.

Raw sequencing reads in the fastq files were mapped with STAR version 2.6.a (*49*). GENCODE release 29, based on the GRCh38 reference genome, and the corresponding GTF file were used. The table of counts was obtained with featureCounts function in the package subread, version 1.6.4. The differential gene expression analysis (DEG) was assessed with voom+limma in the limma package version 3.40.2 and using R version 3.6.0. Raw library size differences between samples were treated with the weighted "trimmed mean method" implemented in the edgeR package. Clustering method used is Ward.D2 with correlation distances and principal components analysis. For the differential expression analysis, read counts were converted to log2 counts per million, and the mean-variance relationship was modeled with precision weights using voom approach in limma package. Raw data are accessible at the NCBI Gene Expression Omnibus (GEO) accession code GSE131286.

Functional analysis of expression data

Intersection of DEG for A673 shRING1B knockdown with those for A673 shEWSR1-FLI1 with accession number GSE61953 (*10*) was obtained by calculating a delta-score as described by the authors. Absolute FC > 1.25 and 1.5 for RING1B and EWSR1-FLI1 datasets were selected, respectively. Overlaps for positive and negative gene sets were obtained using Vennerable R package and BioVenn. Functional analysis of the intersection between RING1B and EWSR1-FLI1 gene lists was performed in Enrichr. Normalized enrichment scores on A673 and SK-ES1 shRING1B versus shCTRL were obtained with GSEA using the Hallmark gene set collection. GSEA was used to analyze enrichment on the list of 983 down-regulated TSG in tumor samples versus normal tissue from TSGene database (*50*) (https://bioinfo.uth.edu/TSGene/). Analysis of expression levels for *AURKB*, *CSNK2A1*, and *MAP2K1* were performed using information from GEO2R GSE7007 for the probes 209464_at, 212075_s_at, and 202670_at, respectively.

Immunohistochemistry

Immunohistochemical analyses were performed following standard techniques. The antibodies used are given in table S6. Tumors were fixed in formalin and embedded in paraffin for subsequent processing. Consecutive, sections were deparaffinized, rehydrated, and heated with Epitope Retrieval Solution (pH 6.0) (Novocastra Laboratories). Reactions were developed with Novolink Polymer Detection System (Novocastra Laboratories). Immunoreactivity was visualized by diaminobenzidine, and nuclei were counterstained with hematoxylin. Tissue was then dehydrated with alcohol, permeated with xylene, and mounted with Permount organic mounting solution (Thermo Fisher Scientific). Images were evaluated by a pathologist to select regions of interest and analyzed with the Dotslide Microscope and Olympia Software (Olympus). Similar regions of every sample were selected from every section.

Chromatin immunoprecipitation followed by quantitative polymerase chain reaction

Cells were treated with 1% formaldehyde at room temperature for 10 min, and the cross-linking reaction was stop by adding 500 μl glycine (1.25 M). Cells were resuspended in lysis buffer [0.1% SDS, 0.15 M NaCl, 1% Triton X-100, 1 mM EDTA, 20 mM tris (pH 8), and protease inhibitors (1 mg/ml)] and sonicated with Bioruptor Pico (Diagenode) for 10 cycles until chromatin was sheared to an average fragment length of 200 bp. After centrifugation, a small fraction of eluted chromatin was measured with Qubit. Starting with 30 μg of sample, immunoprecipitation for each antibody was performed overnight (table S6); 50 μl of Dynabeads Protein A (Invitrogen) was then added and incubated for 2 hours at 4°C under rotation. Immunoprecipitates were washed once with TSE I [0.1% SDS, 1% Triton X-100, 2 mM EDTA, 20 mM tris-HCl (pH 8), and 150 mM NaCl], TSE II [0.1% SDS, 1% Triton X-100, 2 mM EDTA, 20 mM tris-HCl (pH 8), and 500 mM NaCl], and TSE III [0.25 M LiCl, 1% Nonidet P-40, 1% deoxycholate, 1 mM EDTA, and 10 mM tris-HCl (pH 8)] and then twice with tris-EDTA buffer. Washed pellets were eluted with 120 μl of a solution of 1% SDS and 0.1 M $NaHCO_3$. Eluted pellets were decross-linked for 5 hours at 65°C and purified on 50 μl of tris-EDTA buffer with the QIAquick PCR Purification Kit (Qiagen). Differences in the DNA content at each binding region (sequences in table S6) from every immunoprecipitation assay were determined by real-time PCR using the ABI 7700 sequence detection system and SYBR Green master mix protocol (Applied Biosystems). Each immunoprecipitation was done in triplicate, and PCR assays were performed using fixed amounts of input and immunoprecipitated DNA. For every amplicon, standard curves to calculate efficiency and melting curves to confirm single amplicons were obtained. The reported data represent real-time PCR values normalized to input DNA and are expressed as percentage (%) of bound/input signal.

ChIP-seq and bioinformatic analysis

Libraries were prepared using the NEBNext Ultra DNA Library Prep from Illumina according to the manufacturer's protocol. Briefly, 5 ng of input and ChIP-enriched DNA were subjected to end repair and addition of "A" bases to 3′ ends, ligation of adapters, and USER excision. All purification steps were performed using AgenCourt AMPure XP beads (Qiagen). Library amplification was performed by PCR using NEBNext Multiplex Oligos from Illumina. Final libraries were analyzed using Agilent high sensitivity chip to estimate the quantity and to check size distribution and then were quantified by

qPCR using the KAPA Library Quantification Kit (KapaBiosystems) before amplification with Illumina's cBot. Libraries were loaded onto the flow cell sequencer 1 × 50 on Illumina's HiSeq 2500.

ChIP-seq samples were mapped against the hg19 human genome assembly using BowTie with the option –m 1 to discard those reads that could not be uniquely mapped to just one region. A second replicate of RING1B and H2Aub was sequenced to evaluate the statistical significance of the results. Model-based analysis of ChIP-seq (MACS) was run individually on each replicate with the default parameters but with the shift size adjusted to 100 bp to perform the peak calling against the corresponding control sample (*51*). DiffBind was initially run over the peaks reported by MACS for each pair of replicates of the same experiment to generate a consensus set of peaks (*28*). Next, DiffBind was run again over each pair of replicates of the same experiment, samples and inputs, to find the peaks from the consensus set that were significantly enriched in both replicates in comparison to the corresponding controls (categories, DBA_CONDITION; block, DBA_REPLICATE; and method, DBA_DESEQ2_BLOCK). DiffBind RING1B peaks with $P < 0.05$ and H2Aub peaks with $P < 0.05$ and false discovery rate < 0.00001 were selected for further analysis. The genome distribution of each set of peaks was calculated by counting the number of peaks fitted on each class of region according to RefSeq annotations. Promoter is the region between 2.5 kb upstream and 2.5 kb downstream of the TSS. Genic regions correspond to the rest of the gene (the part that is not classified as promoter), and the rest of the genome is considered to be intergenic. Peaks that overlapped with more than one genomic feature were proportionally counted the same number of times. Each set of target genes was retrieved by matching the ChIP-seq peaks in the region 2.5 kb upstream of the TSS until the end of the transcripts as annotated in RefSeq. Reports of functional enrichments of GO categories were generated using the EnrichR tool. Aggregated plots showing the average distribution of ChIP-seq reads around the summit of each peak were generated by counting the number of reads for each region and then averaging the values for the total number of mapped reads of each sample and the total number of peaks in the particular gene set. To perform the comparison between two sets of peaks, a minimum overlap of one nucleotide was necessary to consider one match. The heatmap displaying the density of ChIP-seq reads 5 kb around the summit of each peak set were generated by counting the number of reads in this region for each individual peak and normalizing this value with the total number of mapped reads of the sample. Peaks on each ChIP heatmap were ranked by the logarithm of the average number of reads in the same genomic region. On the other hand, we separated the single peaks of RING1B into distal and TSS (±5 kb around one RefSeq gene) to generate the heatmap of ChIP-seq signal strength of RING1B, EWSR1-FLI1, H3K27me3, H2Aub, and H3K27ac over the two classes of RING1B peaks detected above (distal and TSS). To build our collection of enhancers and promoters, we reanalyzed published ChIP-seq samples of H3K4me1, H3K27ac, H3K27me3, and H3K4me3 in A673 cells (*10*). H3K27ac and H3K27me3 peaks were used to discriminate between active or repressed regulatory regions. Promoters were defined as ChIP peaks of H3K27 found up to 2.5 kb from the TSS of one gene and enhancers on intergenic areas outside promoters or within gene introns. H3K4me3 was required to be present in promoters but absent in enhancers. We defined four classes of regulatory elements: active enhancers (H3K27ac), active promoters (H3K27ac + H3K4me3), poised enhancers (H3K27me3), and bivalent promoters (H3K27me3 + H3K4me3). The MEME-ChIP tool was used to perform motif-finding analysis of the sequences bound by each factor. The UCSC genome browser was used to generate the screenshots of each group of experiments along the manuscript (*52*). Raw data, genome-wide profiles, and peaks of each ChIP-seq experiment are accessible at the NCBI GEO accession code GSE131286.

Chromatin state analysis of EWSR1-FLI1 binding regions

We have determined the composition of 3945 EWSR1-FLI1 biding sites in terms of 15 chromatin states from the segmentations generated by Epigenome Roadmap Consortium (GEO code: GSE61953) for six different cell types: HUVECs (E122), H1 (E003) and H9 ES cells (E008), H1-derived mesenchymal stem cells (E006), BM-derived MSCs (E026), and adipose-derived MSC (E025) (*26*). The statistical significance of the relative frequency of each stage at every cell type was assessed in comparison to the same value measured along the whole genome, using the Fisher's exact test. The R package GenomicRanges from Bioconductor was used for calculations of compositions. Next, to generate the final heatmap, we have grouped certain states for semantic similarity (active TSS category includes active and flanking active TSS states; transcription includes flanking, strong, and weak states; enhancers account for both genic and intergenic; bivalent TSS include also flanking bivalent promoters and PcG repressed include both repressed and weak repressed). Thus, the relative frequencies of the new eight states were recalculated, while quiescent state was discarded from the analysis. Last, the enrichment percentage at a particular stage was calculated as the difference between the relative frequency at the EWSR1-FLI1 ChIP-seq sites minus the relative frequency at the whole genome normalized by the relative frequency at the whole genome again.

Mouse xenograft models

In vivo studies were performed after the approval of the Institutional Animal Research Ethics Committee. Athymic nude mice (Envigo) were injected subcutaneously with 4×10^6 cells for shCTRL#seq1 and shRING1B#seq1 and 2×10^6 for seq#2. shCTRL cells were resuspended in 200 μl of Matrigel (Becton Dickinson) with phosphate-buffered saline and injected into both flanks (5 mice $n = 10$ for seq#1 and 6 mice, $n = 12$ for seq#2). The same procedure was performed for the SK-ES1 shRING1B cell line. Tumor growth was monitored three times a week by measuring tumor volume with a digital caliper. Mice were euthanized when tumors reached a size of 2.5 cm in any dimension. Survival curves were calculated using the Kaplan-Meier method and were compared with a log-rank test. At the end of the experiment, tumors were excised; half of each specimen was frozen in liquid nitrogen for RNA extraction, and the other was fixed in 10% formalin for immunohistochemistry experiments.

SUPPLEMENTARY MATERIALS

Supplementary material for this article is available at http://advances.sciencemag.org/cgi/content/full/6/43/eaba3058/DC1

View/request a protocol for this paper from *Bio-protocol*.

REFERENCES AND NOTES

1. T. G. P. Grünewald, F. Cidre-Aranaz, D. Surdez, E. M. Tomazou, E. de Álava, H. Kovar, P. H. Sorensen, O. Delattre, U. Dirksen, Ewing sarcoma. *Nat. Rev. Dis. Primers.* **4**, 5 (2018).
2. B. D. Crompton, C. Stewart, A. Taylor-Weiner, G. Alexe, K. C. Kurek, M. L. Calicchio, A. Kiezun, S. L. Carter, S. A. Shukla, S. S. Mehta, A. R. Thorner, C. de Torres, C. Lavarino, M. Sunol, A. McKenna, A. Sivachenko, K. Cibulskis, M. S. Lawrence, P. Stojanov, M. Rosenberg, L. Ambrogio, D. Auclair, S. Seepo, B. Blumenstiel, M. DeFelice, I. Imaz-Rosshandler,

Y. C. A. Schwarz-Cruz, M. N. Rivera, C. Rodriguez-Galindo, M. D. Fleming, T. R. Golub, G. Getz, J. Mora, K. Stegmaier, The genomic landscape of pediatric Ewing sarcoma. *Cancer Discov.* **4**, 1326–1341 (2014).
3. N. Riggi, M.-L. Suvà, D. Suva, L. Cironi, P. Provero, S. Tercier, J.-M. Joseph, J.-C. Stehle, K. Baumer, V. Kindler, I. Stamenkovic, EWS-FLI-1 expression triggers a Ewing's sarcoma initiation program in primary human mesenchymal stem cells. *Cancer Res.* **68**, 2176–2185 (2008).
4. F. Tirode, K. Laud-Duval, A. Prieur, B. Delorme, P. Charbord, O. Delattre, Mesenchymal stem cell features of Ewing tumors. *Cancer Cell* **11**, 421–429 (2007).
5. C. von Levetzow, X. Jiang, Y. Gwye, G. von Levetzow, L. Hung, A. Cooper, J. H.-R. Hsu, E. R. Lawlor, Modeling initiation of Ewing sarcoma in human neural crest cells. *PLOS ONE* **6**, e19305 (2011).
6. O. Delattre, J. Zucman, B. Plougastel, C. Desmaze, T. Melot, M. Peter, H. Kovar, I. Joubert, P. de Jong, G. Rouleau, A. Aurias, G. Thomas, Gene fusion with an *ETS* DNA-binding domain caused by chromosome translocation in human tumours. *Nature* **359**, 162–165 (1992).
7. S. Sankar, R. Bell, B. Stephens, R. Zhuo, S. Sharma, D. J. Bearss, S. L. Lessnick, Mechanism and relevance of EWS/FLI-mediated transcriptional repression in Ewing sarcoma. *Oncogene* **32**, 5089–5100 (2013).
8. K. Gangwal, S. Sankar, P. C. Hollenhorst, M. Kinsey, S. C. Haroldsen, A. A. Shah, K. M. Boucher, W. S. Watkins, L. B. Jorde, B. J. Graves, S. L. Lessnick, Microsatellites as EWS/FLI response elements in Ewing's sarcoma. *Proc. Natl. Acad. Sci. U.S.A.* **105**, 10149–10154 (2008).
9. N. Guillon, F. Tirode, V. Boeva, A. Zynovyev, E. Barillot, O. Delattre, The oncogenic EWS-FLI1 protein binds in vivo GGAA microsatellite sequences with potential transcriptional activation function. *PLOS ONE* **4**, e4932 (2009).
10. N. Riggi, B. Knoechel, S. M. Gillespie, E. Rheinbay, G. Boulay, M. L. Suva, N. E. Rossetti, W. E. Boonseng, O. Oksuz, E. B. Cook, A. Formey, A. Patel, M. Gymrek, V. Thapar, V. Deshpande, D. T. Ting, F. J. Hornicek, G. P. Nielsen, I. Stamenkovic, M. J. Aryee, B. E. Bernstein, M. N. Rivera, EWS-FLI1 utilizes divergent chromatin remodeling mechanisms to directly activate or repress enhancer elements in Ewing sarcoma. *Cancer Cell* **26**, 668–681 (2014).
11. E. M. Tomazou, N. C. Sheffield, C. Schmidl, M. Schuster, A. Schonegger, P. Datlinger, S. Kubicek, C. Bock, H. Kovar, Epigenome mapping reveals distinct modes of gene regulation and widespread enhancer reprogramming by the oncogenic fusion protein EWS-FLI1. *Cell Rep.* **10**, 1082–1095 (2015).
12. G. Boulay, G. J. Sandoval, N. Riggi, S. Iyer, R. Buisson, B. Naigles, M. E. Awad, S. Rengarajan, A. Volorio, M. J. McBride, L. C. Broye, L. Zou, I. Stamenkovic, C. Kadoch, M. N. Rivera, Cancer-specific retargeting of BAF complexes by a prion-like domain. *Cell* **171**, 163–178. e19 (2017).
13. S. Aranda, G. Mas, L. Di Croce, Regulation of gene transcription by Polycomb proteins. *Sci. Adv.* **1**, e1500737 (2015).
14. K. Rai, K. C. Akdemir, L. N. Kwong, P. Fiziev, C.-J. Wu, E. Z. Keung, S. Sharma, N. S. Samant, M. Williams, J. B. Axelrad, A. Shah, D. Yang, E. A. Grimm, M. C. Barton, D. R. Milton, T. P. Heffernan, J. W. Horner, S. Ekmekcioglu, A. J. Lazar, J. Ernst, L. Chin, Dual roles of RNF2 in melanoma progression. *Cancer Discov.* **5**, 1314–1327 (2015).
15. Z. Gao, P. Lee, J. M. Stafford, M. von Schimmelmann, A. Schaefer, D. Reinberg, An AUTS2-Polycomb complex activates gene expression in the CNS. *Nature* **516**, 349–354 (2014).
16. G. H. Richter, S. Plehm, A. Fasan, S. Rössler, R. Unland, I. M. Bennani-Baiti, M. Hotfilder, D. Löwel, I. von Luettichau, I. Mossbrugger, L. Quintanilla-Martinez, H. Kovar, M. S. Staege, C. Müller-Tidow, S. Burdach, EZH2 is a mediator of EWS/FLI1 driven tumor growth and metastasis blocking endothelial and neuro-ectodermal differentiation. *Proc. Natl. Acad. Sci. U.S.A.* **106**, 5324–5329 (2009).
17. D. Douglas, J. H.-R. Hsu, L. Hung, A. Cooper, D. Abdueva, J. van Doorninck, G. Peng, H. Shimada, T. J. Triche, E. R. Lawlor, BMI-1 promotes Ewing sarcoma tumorigenicity independent of CDKN2A repression. *Cancer Res.* **68**, 6507–6515 (2008).
18. I. Hernandez-Muñoz, E. Figuerola, S. Sanchez-Molina, E. Rodriguez, A. I. Fernández-Mariño, C. Pardo-Pastor, M. I. Bahamonde, J. M. Fernández-Fernández, D. J. García-Domínguez, L. Hontecillas-Prieto, C. Lavarino, A. M. Carcaboso, C. de Torres, O. M. Tirado, E. de Alava, J. Mora, RING1B contributes to Ewing sarcoma development by repressing the NaV1.6 sodium channel and the NF-κB pathway, independently of the fusion oncoprotein. *Oncotarget* **7**, 46283–46300 (2016).
19. M. Patel, J. M. Simon, M. D. Iglesia, S. B. Wu, A. W. McFadden, J. D. Lieb, I. J. Davis, Tumor-specific retargeting of an oncogenic transcription factor chimera results in dysregulation of chromatin and transcription. *Genome Res.* **22**, 259–270 (2012).
20. L. K. Svoboda, A. Harris, N. J. Bailey, R. Schwentner, E. Tomazou, C. von Levetzow, B. Magnuson, M. Ljungman, H. Kovar, E. R. Lawlor, Overexpression of HOX genes is prevalent in Ewing sarcoma and is associated with altered epigenetic regulation of developmental transcription programs. *Epigenetics* **9**, 1613–1625 (2014).
21. N. Riggi, M.-L. Suvà, C. De Vito, P. Provero, J.-C. Stehle, K. Baumer, L. Cironi, M. Janiszewska, T. Petricevic, D. Suva, S. Tercier, J.-M. Joseph, L. Guillou, I. Stamenkovic, EWS-FLI-1 modulates miRNA145 and SOX2 expression to initiate mesenchymal stem cell reprogramming toward Ewing sarcoma cancer stem cells. *Genes Dev.* **24**, 916–932 (2010).
22. M. S. Staege, C. Hutter, I. Neumann, S. Foja, U. E. Hattenhorst, G. Hansen, D. Afar, S. E. G. Burdach, DNA microarrays reveal relationship of Ewing family tumors to both endothelial and fetal neural crest-derived cells and define novel targets. *Cancer Res.* **64**, 8213–8221 (2004).
23. R. Smith, L. A. Owen, D. J. Trem, J. S. Wong, J. S. Whangbo, T. R. Golub, S. L. Lessnick, Expression profiling of EWS/FLI identifies NKX2.2 as a critical target gene in Ewing's sarcoma. *Cancer Cell* **9**, 405–416 (2006).
24. O. M. Tirado, S. Mateo-Lozano, J. Villar, L. E. Dettin, A. Llort, S. Gallego, J. Ban, H. Kovar, V. Notario, Caveolin-1 (CAV1) is a target of EWS/FLI-1 and a key determinant of the oncogenic phenotype and tumorigenicity of Ewing's sarcoma cells. *Cancer Res.* **66**, 9937–9947 (2006).
25. K. E. Ryland, A. G. Hawkins, D. J. Weisenberger, V. Punj, S. C. Borinstein, P. W. Laird, J. R. Martens, E. R. Lawlor, Promoter methylation analysis reveals That KCNA5 ion channel silencing supports Ewing sarcoma cell proliferation. *Mol. Cancer Res.* **14**, 26–34 (2016).
26. Roadmap Epigenomics Consortium, A. Kundaje, W. Meuleman, J. Ernst, M. Bilenky, A. Yen, A. Heravi-Moussavi, P. Kheradpour, Z. Zhang, J. Wang, M. J. Ziller, V. Amin, J. W. Whitaker, M. D. Schultz, L. D. Ward, A. Sarkar, G. Quon, R. S. Sandstrom, M. L. Eaton, Y.-C. Wu, A. R. Pfenning, X. Wang, M. Claussnitzer, Y. Liu, C. Coarfa, R. A. Harris, N. Shoresh, C. B. Epstein, E. Gjoneska, D. Leung, W. Xie, R. D. Hawkins, R. Lister, C. Hong, P. Gascard, A. J. Mungall, R. Moore, E. Chuah, A. Tam, T. K. Canfield, R. S. Hansen, R. Kaul, P. J. Sabo, M. S. Bansal, A. Carles, J. R. Dixon, K.-H. Farh, S. Feizi, R. Karlic, A.-R. Kim, A. Kulkarni, D. Li, R. Lowdon, G. Elliott, T. R. Mercer, S. J. Neph, V. Onuchic, P. Polak, N. Rajagopal, P. Ray, R. C. Sallari, K. T. Siebenthall, N. A. Sinnott-Armstrong, M. Stevens, R. E. Thurman, J. Wu, B. Zhang, X. Zhou, A. E. Beaudet, L. A. Boyer, P. L. De Jager, P. J. Farnham, S. J. Fisher, D. Haussler, S. J. Jones, W. Li, M. A. Marra, M. T. McManus, S. Sunyaev, J. A. Thomson, T. D. Tlsty, L.-H. Tsai, W. Wang, R. A. Waterland, M. Q. Zhang, L. H. Chadwick, B. E. Bernstein, J. F. Costello, J. R. Ecker, M. Hirst, A. Meissner, A. Milosavljevic, B. Ren, J. A. Stamatoyannopoulos, T. Wang, M. Kellis, Integrative analysis of 111 reference human epigenomes. *Nature* **518**, 317–330 (2015).
27. H. L. Chan, F. Beckedorff, Y. Zhang, J. Garcia-Huidobro, H. Jiang, A. Colaprico, D. Bilbao, M. E. Figueroa, J. LaCava, R. Shiekhattar, L. Morey, Polycomb complexes associate with enhancers and promote oncogenic transcriptional programs in cancer through multiple mechanisms. *Nat. Commun.* **9**, 3377 (2018).
28. C. S. Ross-Innes, R. Stark, A. E. Teschendorff, K. A. Holmes, H. R. Ali, M. J. Dunning, G. D. Brown, O. Gojis, I. O. Ellis, A. R. Green, S. Ali, S.-F. Chin, C. Palmieri, C. Caldas, J. S. Carroll, Differential oestrogen receptor binding is associated with clinical outcome in breast cancer. *Nature* **481**, 389–393 (2012).
29. E. Blanco, M. Gonzalez-Ramirez, A. Alcaine-Colet, S. Aranda, L. Di Croce, The bivalent genome: Characterization, structure, and regulation. *Trends Genet.* **36**, 118–131 (2020).
30. E. M. Mendenhall, R. P. Koche, T. Truong, V. W. Zhou, B. Issac, A. S. Chi, M. Ku, B. E. Bernstein, GC-rich sequence elements recruit PRC2 in mammalian ES cells. *PLOS Genet.* **6**, e1001244 (2010).
31. V. Di Carlo, I. Mocavini, L. Di Croce, Polycomb complexes in normal and malignant hematopoiesis. *J. Cell Biol.* **218**, 55–69 (2019).
32. G.-A. Franzetti, K. Laud-Duval, W. van der Ent, A. Brisac, M. Irondelle, S. Aubert, U. Dirksen, C. Bouvier, G. de Pinieux, E. Snaar-Jagalska, P. Chavrier, O. Delattre, Cell-to-cell heterogeneity of EWSR1-FLI1 activity determines proliferation/migration choices in Ewing sarcoma cells. *Oncogene* **36**, 3505–3514 (2017).
33. Q. Cao, X. Wang, M. Zhao, R. Yang, R. Malik, Y. Qiao, A. Poliakov, A. K. Yocum, Y. Li, W. Chen, X. Cao, X. Jiang, A. Dahiya, C. Harris, F. Y. Feng, S. Kalantry, Z. S. Qin, S. M. Dhanasekaran, A. M. Chinnaiyan, The central role of EED in the orchestration of polycomb group complexes. *Nature Commun.* **5**, 3127 (2014).
34. D. J. García-Domínguez, L. Hontecillas-Prieto, E. A. León, S. Sánchez-Molina, P. Rodríguez-Núñez, F. J. Morón, N. Hajji, C. Mackintosh, E. de Álava, An inducible ectopic expression system of EWSR1-FLI1 as a tool for understanding Ewing sarcoma oncogenesis. *PLOS ONE* **15**, e0234243 (2020).
35. L. Cironi, N. Riggi, P. Provero, N. Wolf, M.-L. Suvà, D. Suva, V. Kindler, I. Stamenkovic, IGF1 is a common target gene of Ewing's sarcoma fusion proteins in mesenchymal progenitor cells. *PLOS ONE* **3**, e2634 (2008).
36. A. Frangini, M. Sjöberg, M. Roman-Trufero, G. Dharmalingam, V. Haberle, T. Bartke, B. Lenhard, M. Malumbres, M. Vidal, N. Dillon, The aurora B kinase and the polycomb protein ring1B combine to regulate active promoters in quiescent lymphocytes. *Mol. Cell* **51**, 647–661 (2013).
37. K. Wakahara, T. Ohno, M. Kimura, T. Masuda, S. Nozawa, T. Dohjima, T. Yamamoto, A. Nagano, G. Kawai, A. Matsuhashi, M. Saitoh, I. Takigami, Y. Okano, K. Shimizu, EWS-Fli1 up-regulates expression of the Aurora A and Aurora B kinases. *Mol. Cancer Res.* **6**, 1937–1945 (2008).
38. B. A. Teicher, E. Polley, M. Kunkel, D. Evans, T. Silvers, R. Delosh, J. Laudeman, C. Ogle, R. Reinhart, M. Selby, J. Connelly, E. Harris, A. Monks, J. Morris, Sarcoma cell line screen of oncology drugs and investigational agents identifies patterns associated with gene and microRNA expression. *Mol. Cancer Ther.* **14**, 2452–2462 (2015).

39. G. Boulay, A. Volorio, S. Iyer, L. C. Broye, I. Stamenkovic, N. Riggi, M. N. Rivera, Epigenome editing of microsatellite repeats defines tumor-specific enhancer functions and dependencies. *Genes Dev.* **32**, 1008–1019 (2018).
40. S. L. Kloet, M. M. Makowski, H. I. Baymaz, L. van Voorthuijsen, I. D. Karemaker, A. Santanach, P. W. T. C. Jansen, L. Di Croce, M. Vermeulen, The dynamic interactome and genomic targets of Polycomb complexes during stem-cell differentiation. *Nat. Struct. Mol. Biol.* **23**, 682–690 (2016).
41. A. Banito, X. Li, A. N. Laporte, J.-S. Roe, F. Sanchez-Vega, C.-H. Huang, A. R. Dancsok, K. Hatzi, C.-C. Chen, D. F. Tschaharganeh, R. Chandwani, N. Tasdemir, K. B. Jones, M. R. Capecchi, C. R. Vakoc, N. Schultz, M. Ladanyi, T. O. Nielsen, S. W. Lowe, The SS18-SSX oncoprotein hijacks KDM2B-PRC1.1 to drive synovial sarcoma. *Cancer Cell* **34**, 346–348 (2018).
42. V. van den Boom, H. Maat, M. Geugien, A. Rodríguez López, A. M. Sotoca, J. Jaques, A. Z. Brouwers-Vos, F. Fusetti, R. W. Groen, H. Yuan, A. C. Martens, H. G. Stunnenberg, E. Vellenga, J. H. Martens, J. J. Schuringa, Non-canonical PRC1.1 targets active genes independent of H3K27me3 and is essential for leukemogenesis. *Cell Rep.* **14**, 332–346 (2016).
43. Z. Wang, M. D. Gearhart, Y. W. Lee, I. Kumar, B. Ramazanov, Y. Zhang, C. Hernandez, A. Y. Lu, N. Neuenkirchen, J. Deng, J. Jin, Y. Kluger, T. A. Neubert, V. J. Bardwell, N. B. Ivanova, A non-canonical BCOR-PRC1.1 complex represses differentiation programs in human ESCs. *Cell Stem Cell* **22**, 235–251.e9 (2018).
44. B. E. Gryder, M. E. Yohe, H.-C. Chou, X. Zhang, J. Marques, M. Wachtel, B. Schaefer, N. Sen, Y. Song, A. Gualtieri, S. Pomella, R. Rota, A. Cleveland, X. Wen, S. Sindiri, J. S. Wei, F. G. Barr, S. Das, T. Andresson, R. Guha, M. Lal-Nag, M. Ferrer, J. F. Shern, K. Zhao, C. J. Thomas, J. Khan, PAX3–FOXO1 establishes myogenic super enhancers and confers BET bromodomain vulnerability. *Cancer Discov.* **7**, 884–899 (2017).
45. A. Puissant, S. M. Frumm, G. Alexe, C. F. Bassil, J. Qi, Y. H. Chanthery, E. A. Nekritz, R. Zeid, W. C. Gustafson, P. Greninger, M. J. Garnett, U. McDermott, C. H. Benes, A. L. Kung, W. A. Weiss, J. E. Bradner, K. Stegmaier, Targeting MYCN in neuroblastoma by BET bromodomain inhibition. *Cancer Discov.* **3**, 308–323 (2013).
46. P. N. Gollavilli, A. Pawar, K. Wilder-Romans, R. Natesan, C. G. Engelke, V. L. Dommeti, P. M. Krishnamurthy, A. Nallasivam, I. J. Apel, T. Xu, Z. S. Qin, F. Y. Feng, I. A. Asangani, EWS/ETS-driven Ewing sarcoma requires BET bromodomain proteins. *Cancer Res.* **78**, 4760–4773 (2018).
47. G. E. Winter, U. Rix, A. Lissat, A. Stukalov, M. K. Mullner, K. L. Bennett, J. Colinge, S. M. Nijman, S. Kubicek, H. Kovar, U. Kontny, G. Superti-Furga, An integrated chemical biology approach identifies specific vulnerability of Ewing's sarcoma to combined inhibition of Aurora kinases A and B. *Mol. Cancer Ther.* **10**, 1846–1856 (2011).
48. S. Wang, E. E. Hwang, R. Guha, A. F. O'Neill, N. Melong, C. J. Veinotte, A. C. Saur, K. Wuerthele, M. Shen, C. McKnight, G. Alexe, M. E. Lemieux, A. Wang, E. Hughes, X. Xu, M. B. Boxer, M. D. Hall, A. Kung, J. N. Berman, M. I. Davis, K. Stegmaier, B. D. Crompton, High-throughput chemical screening identifies focal adhesion kinase and Aurora kinase B inhibition as a synergistic treatment combination in Ewing sarcoma. *Clin. Cancer Res.* **25**, 4552–4566 (2019).
49. A. Dobin, C. A. Davis, F. Schlesinger, J. Drenkow, C. Zaleski, S. Jha, P. Batut, M. Chaisson, T. R. Gingeras, STAR: Ultrafast universal RNA-seq aligner. *Bioinformatics* **29**, 15–21 (2013).
50. M. Zhao, J. Sun, Z. Zhao, TSGene: A web resource for tumor suppressor genes. *Nucleic Acids Res.* **41**, D970–D976 (2013).
51. Y. Zhang, T. Liu, C. A. Meyer, J. Eeckhoute, D. S. Johnson, B. E. Bernstein, C. Nusbaum, R. M. Myers, M. Brown, W. Li, X. S. Liu, Model-based analysis of ChIP-Seq (MACS). *Genome Biol.* **9**, R137 (2008).
52. W. J. Kent, C. W. Sugnet, T. S. Furey, K. M. Roskin, T. H. Pringle, A. M. Zahler, D. Haussler, The human genome browser at UCSC. *Genome Res.* **12**, 996–1006 (2002).

Acknowledgments: We thank N. Riggi for reagents and technical advice and M. Martínez-Balbás for technical advice and critical reading of the manuscript. We also thank G. Pascual-Pasto, S. Mateo, and M. Suñol for technical advice, S. Perez-Jaume for statistical advice, and L. Nonell from the Microarray Analysis Service, Hospital del Mar Medical Research Institute (IMIM, Barcelona) for technical advice. Last, we are grateful to the Band of Parents at Hospital Sant Joan de Déu for supporting the overall research activities of the developmental tumor laboratory, PCCB. **Funding:** S.S.-M. and the project were supported by the Spanish Association Against Cancer (AECC) consolidated groups grant (GCB13131578) consortium. The project also had the support from the Asociacion Pablo Ugarte (APU). E.F.-B. was supported by the Spanish government grant, Instituto de Salud Carlos III (PI16/00245) to J.M. The work in the Di Croce laboratory was supported by grants from the Spanish of Economy, Industry and Competitiveness (MEIC) (BFU2016-75008-P), and Fundacion Vencer El Cancer (VEC). **Author contributions:** S.S.-M., L.D.C., and J.M. designed the study, conducted experiments, and wrote the manuscript. J.M. supervised all the work. S.S.-M., E.F.-B., M.S.-J., P.T., C.B., E.P., L.H.-P., and D.J.G.-D. performed the experiments. E.B. and S.G. performed all the bioinformatic analysis. I.H.-M., O.M.T., A.M.C., C.L., and E.Á. provided expertise and feedback. All authors reviewed the manuscript. **Competing interests:** The authors declare that they have no competing interests. **Data and materials availability:** All data needed to evaluate the conclusions in the paper are present in the paper and/or the Supplementary Materials. Additional data related to this paper may be requested from the authors.

Submitted 3 December 2019
Accepted 9 September 2020
Published 23 October 2020
10.1126/sciadv.aba3058

Citation: S. Sánchez-Molina, E. Figuerola-Bou, E. Blanco, M. Sánchez-Jiménez, P. Táboas, S. Gómez, C. Ballaré, D. J. García-Domínguez, E. Prada, L. Hontecillas-Prieto, Á. M. Carcaboso, Ó. M. Tirado, I. Hernández-Muñoz, E. de Álava, C. Lavarino, L. Di Croce, J. Mora, RING1B recruits EWSR1-FLI1 and cooperates in the remodeling of chromatin necessary for Ewing sarcoma tumorigenesis. *Sci. Adv.* **6**, eaba3058 (2020).

ScienceAdvances

RING1B recruits EWSR1-FLI1 and cooperates in the remodeling of chromatin necessary for Ewing sarcoma tumorigenesis

Sara Snchez-Molina, Elisabet Figuerola-Bou, Enrique Blanco, Mara Snchez-Jimnez, Pablo Tboas, Soledad Gmez, Cecilia Ballar, Daniel J. Garca-Domnguez, Estela Prada, Lourdes Hontecillas-Prieto, ngel M. Carcaboso, scar M. Tirado, Inmaculada Hernndez-Muoz, Enrique de lava, Cinzia Lavarino, Luciano Di Croce, and Jaume Mora

Sci. Adv., **6** (43), eaba3058.
DOI: 10.1126/sciadv.aba3058